Research Signpost
37/661 (2), Fort P.O., Trivandrum-695 023, Kerala, India

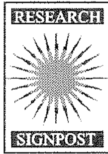

Vacuum Science and Technology: Nitrides as seen by the technology, 2002 ISBN : 81-7736-198-8
Editors : Tanya Paskova and Bo Monemar

15 The molecular beam epitaxy of cubic III-nitrides

D. Schikora, D.J. As and K. Lischka
University of Paderborn, Department of Physics, D-33098 Paderborn

Abstract

Molecular beam epitaxy has successfully been used to grow crystalline layers of group III-nitrides (GaN, AlN and InN) with cubic (zinc-blende) structure. In this article, we discuss these efforts that, despite inherent difficulties due to the metastability of the c-III nitrides, led to substantial improvements of the structural, electrical and optical quality of these wide gap semiconductors. We review experimental work concerned with the epitaxy of c-GaN on various substrates and the control of the growth process in-situ, the important issue of p- and n-type doping of c-GaN and investigations of the structural and optical properties of c-InGaN revealing the importance of composition variations in this material for the understanding of its optical emission.

1. Introduction

Due to their inherent physical properties group III-nitrides (GaN, AlN, InN) find enormous application

Correspondence/Reprint request: Dr. K. Lischka, University of Paderborn, Fachbereich Physik, Warburger Str. 100, D-33095 Paderborn, Germany. E-mail:lischka@physik.uni-paderborn.de

in short wavelength optoelectronic devices and high temperature electronics. In the last years tremendous research efforts have been taken to grow these semiconductors in high quality by various growth methods.

Most of the activity has been devoted to III-nitrides with hexagonal (wurtzite) crystal structure, which is the thermodynamically stable configuration of these compounds. However, the III-nitrides can also exist in the cubic (zinc-blende) structure, which has only a slightly higher (in the order of 10 meV/atom) structural energy, due to the same next neighbour configuration and the ionic character of the bonds [1]. The growth of cubic III-nitrides was strongly motivated by some advantageous properties, which are all linked to their crystal structure. These are: a smaller electron and hole effective mass and an easier access to p-type doping, a higher saturated electron drift velocity and the possibility to produce laser facets by simple cleavage. However, in order to exploit their potential for practical applications, the metastable cubic III-nitrides have to be synthesized in sufficient good quality.

In this review we summarize the achievements, which have been reached in the last years by a growing number of research groups with the Molecular Beam Epitaxy (MBE) of cubic III-nitrides.

2. Molecular beam epitaxy of cubic GaN

The metastable nature of the cubic phase requires growth techniques, which are operating under far from equilibrium conditions. Using MBE, which is known as nonequilibrium growth method, it has been proven by a number of researchers that c-GaN, AlGaN and InGaN of good crystalline quality can be grown [2-20]. For the epitaxial growth, various requirements have to be fulfilled simultaneously, namely, the structural integrity between the nitride layer and the substrate, the nucleation, the adjustment and the maintenance of optimum growth conditions in particular the surface stoichiometry and the substrate temperature.

2.1. Substrates

The first important issue of the growth of cubic nitrides is the choice of appropriate substrates, which are suitable for crystalline nucleation and growth. So far, 3C-SiC [2,12, 13,21-25], GaAs [3,4,6,8-10,14-17,20,26-31], Si [5,7,32], GaP [19], InAs [27], and MgO [11] have been used as substrates. All these substrates were used in orientations having 4-fold symmetry, which is obviously an essential requirement for the epitaxy of metastable cubic GaN. The metric misfit among these materials varies from 20% (GaAs/c-GaN) to -3.5% (3C-SiC/ c-GaN).

Despite the large misfit and the unavoidable tendency of the formation of hexagonal phase material, crystalline growth of cubic GaN could be obtained reproducibly. This is a first surprising and interesting result, because it is well known from growth theory that for lattice mismatch exceeding 14% interface dislocations cannot be defined anymore and coherence between the substrate and the layer is lost. The substrate materials, their lattice mismatch to c-GaN and various growth parameters are listed in Table 1.

The most frequently used substrate material for c-GaN is GaAs because of its commercial availability, the well known surface preparation procedures and the possibility to generate cleaved facets. Silicon substrates also offer important advantages, which are high surface quality, well established preparation and processing procedures

Table 1. Some important parameters of the MBE of c-GaN.

substrate material	lattice mismatch to c-GaN %]	$T_{nucleation}$ [°C]	T_{growth} [°C]	epitaxial relation	Ref.
GaAs	20.0	400-600	600-720	(001)GaAs//(001)GaN [110]GaAs//[110]GaN	[3,4,31] [36, 169]
GaP	17.1	620	700	(001)GaP//(001)GaN [110]GaP//[110]GaN	[19]
Si	16.8	400/650	600/650	(001)Si //(001) GaN [001]Si // [001] GaN	[7, 32]
MgO	-7.2	450	700	(001)MgO//(001)GaN [001]MgO//[001]GaN	[11]
3C-SiC	-3.7	400-500	600-800	(001)SiC //(001)GaN [001]SiC//[001]GaN	[25]

and high thermal stability and conductivity. However, both substrate materials exhibit a very large lattice mismatch to c-GaN and besides this, the use of Si is connected with the common problems of the epitaxy of polar materials on non-polar surfaces.

The cubic modification of SiC (3C-SiC) has the smallest lattice mismatch to c-GaN and therefore seems to be a promising choice to overcome the problems of growing highly mismatched heterostructures. Also the high thermal stability and conductivity of 3C-SiC are advantages. In fact, this material has been proposed first by Pankove [33] for the epitaxy of c-GaN. 3C-SiC layers are usually prepared by various CVD-methods on Si substrates. For the use as substrates in c-GaN heteroepitaxy, the 3C-SiC layers should be relatively thick (3 μm) in order to reduce their defect density. However, that means that the problem to overcome the extraordinary large mismatch is merely shifted from the growth of GaN on Si to the 3C-SiC on Si epitaxy. The attempts of the semiconductor industry to produce 3C-SiC on Si have been stopped few years ago because of inherent difficulties. Therefore, the availability of this material presently is quite low.

The use of GaP as substrate material is connected with the same problems discussed above and has been reported by T.S.Cheng *et al.* [19] MgO substrates were used first by R.C.Powell *et al.* [11] to grow crystalline c-GaN by MBE. The main disadvantage of MgO is the poor conductivity and surface quality and therefore it has been used rarely.

A common feature of all growth experiments reported so far was the use of a low temperature nucleation layer, which was grown at temperature about 100-200°C below the optimum growth temperature of c-GaN. Low growth temperatures basically increase the supersaturation and thus the resulting nucleation density. An almost completely covered substrate surface is expected to result in a smooth and homogenous interface morphology, which is a prerequisite for the growth of high quality GaN layers [7].

The optimum temperatures for the growth of c-GaN on different substrates are all within a narrow range at about 680-740°C. This is significantly lower than the growth temperatures reported for MOCVD of hexagonal GaN, which are 950-1100°C. An analysis of the thermodynamic conditions for physical vapour deposition (PVD) of various semiconductors showed that the optimum growth temperature is closely correlated with the boiling temperature of the layer material [34]. A remarkable result of

this study is the conclusion that the optimum growth temperature is about one third of the boiling temperature. This relation seems reasonable because supersaturation and diffusion are determined by transition enthalpies, which are correlated. Applied to GaN, which has a melting temperature of about 2400°C an optimum growth temperature of about 800°C can be estimated. On the other hand, it has to be considered that the thermal decomposition of the c-GaN surface starts at temperatures above 800°C, characterized by an initially congruent and at higher temperatures incongruent evaporation of surface atoms [35].

According to these thermodynamic prerequisites, it can be assumed that epitaxial growth of c-GaN at temperatures at or slightly above 800°C can be performed under conditions near a dynamic evaporation-condensation equilibrium, where in particular displaced surface atoms have a much larger probability to re-evaporate. If the surface mobility of one species involved is rather low, as it is known from the nitrides, such a growth regime offers some advantages with respect to crystalline perfection.

Okumura *et al.* [25] reported the MBE growth of c-GaN on 3C-SiC substrates at 800°C. Using an additional As-flux (p_{As}~10^{-8} Torr) to stabilise the zinc-blende structure, they found a remarkable improvement of the layer crystallinity as compared to lower growth temperatures of about 650°C. The photoluminescence (PL) spectra of layers grown at 800°C show sharp and intense excitonic emission at 3.27 eV, revealing the high quality of the c-GaN epilayers. In addition, Secondary Ion Mass Spectrometry (SIMS) showed that no significant amount of As is incorporated into the layers, which underlines the role of As as an surfactant in the growth process at 800°C. It is evident that high growth temperatures can only be realized with thermal stable substrates like 3C-SiC, Si and MgO. The most frequently used GaAs-substrates do not allow substrate temperatures of about 800°C, due to the strong loss of As and the resulting decomposition of the substrate during growth. Therefore, the optimum growth temperatures for c-GaN on GaAs substrates given in the literature [3,4,6,8-10,14-17,20,27-31,36] of about 680-720°C are clearly below of the estimated thermodynamic optimum. They are obviously a compromise between the crystalline perfection of c-GaN and the substrate stability.

In most cases the MBE of c-GaN on GaAs was initiated on a (2x4) reconstructed (001) GaAs surface. This growth orientation allows to prepare laser facets by cleaving. A typical growth procedure, which was described among others by Brandt *et al.* [20] consists of two steps. As a first step a low temperature buffer layer with a thickness of about 10 nm was grown at about 600°C. Then the substrate temperature was ramped up to 680-740°C and the layer growth was continued using carefully controlled stoichiometric conditions.

The preparation of 3C-SiC surfaces was described in Refs. 2,12,37,38. Usually, the SiC-coated Si wafers were etched in an HF solution to remove oxide layers and, after loading into the growth chamber, thermally cleaned at 750-900°C for approximately 10-30 min before the nucleation was started.

The pre-treatment of Si-substrates is quite similar to that of 3C-SiC. Cleaning in different solvents, etching in HF-solutions and annealing at 750-850°C for 15-30 min in vacuum or H_2-atmosphere were reported in the literature. [5, 7,32] The growth procedure of GaN on 3C-SiC and Si-substrates is analogous to that on GaAs substrates. A low temperature nucleation layer is grown first, followed by high temperature layer growth as indicated in Table 1.

The growth rates reported for optimized conditions are 0.1-0.4 ML/s [26]. The dependence of the c-GaN growth rate on the Ga-flux is shown in Fig. 1. Under conditions of N-excess the growth rate increases linearly with increasing Ga-flux expressed as Ga-cell temperature. At a certain Ga/N - flux ratio the growth rate shows a maximum value, which cannot be increased by further increase of the Ga-flux. The rate limiting component under Ga-excess conditions is the N-flux, which was kept constant in these experiments. The dashed line characterises the transition from N-excess to Ga-excess conditions, which plays a decisive role in the control of the phase purity and the structural quality of c-GaN layers. The respective activation energy of about 2.8 eV was obtained from an Arrhenius plot of the growth rate. It is in good agreement with the value found for evaporation of liquid Gallium. This confirms the assumption that the c-GaN growth is controlled by the incoming Ga-flux at substrate temperatures of about 620°C and under N-excess conditions, e.g. a thermodynamically controlled growth regime can be established at least for the low temperature growth stage.

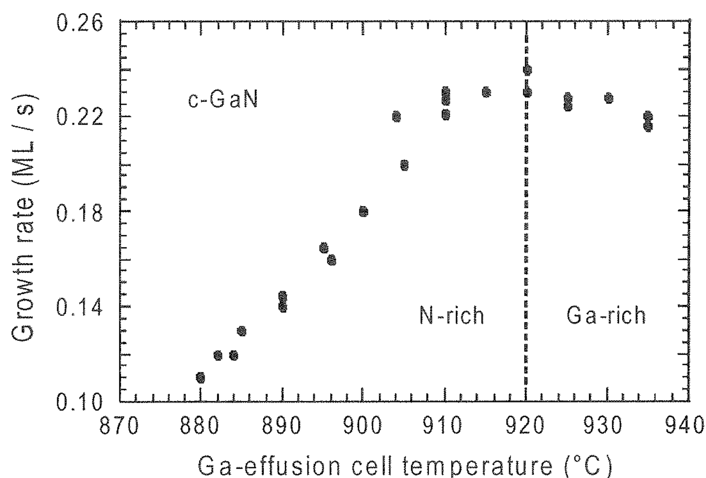

Figure 1. Dependence of the c-GaN growth rate on the Ga-effusion cell temperature. The Nitrogen-flux and the substrate temperature (T_s = 620°C) are constant.

A crucial prerequisite for the MBE of c-GaN was the development of new and efficient sources for nitrogen effusion. Basically there are two different approaches to generate Nitrogen atoms, which are needed in epitaxial growth:

(i) Cracking of the N-N bond in Nitrogen molecules, which is one of the strongest in nature, by appropriate plasma techniques.

(ii) Use of nitrogen containing gases with relatively weak Nitrogen- to- radical bond strength, like NH_3 (ammonia) or Hy- (hydrazine) derivates like DMHy (Dimethylhydrazine) or MMHy (Monomethylhydrazine).

The first approach leads to plasma-enhanced MBE, which does not change the character of MBE as a physical deposition method. It is a promising technique to grow c-GaN. Principally, either electron cyclotron resonance (ECR) or radio frequency (RF)

plasma methods are used to obtain excited nitrogen. So far, many groups have reported on electrical and optical properties of plasma-enhanced MBE grown GaN layers [39-41]. A systematic comparison of the properties and the plasma composition of ECR and RF plasmas was published recently by Cho *et al.* [42]. It was found by Quadrupol Mass Spectroscopy (QMS) measurements that in the ECR plasma the intensity of molecular nitrogen was higher than the intensity of atomic nitrogen and both intensities were increasing with increasing nitrogen pressure. In contrast to that the intensity of atomic nitrogen in the RF plasma was always higher than that of molecular nitrogen and the ratio between atomic-and molecular nitrogen was increasing with increasing nitrogen pressure. The ECR plasma contains more highly excited atomic nitrogen and molecular nitrogen as compared to RF plasma, where the atomic nitrogen is in the ground state and excited nitrogen is in lower excited states. It was concluded that the optimum growth window for c-GaN MBE is here narrower as for plasma. However no deep emission in PL spectra was obtained by using rf plasma sources. We have found in own QMS-studies that in dependence on the flow rate and the rf power applied, the content of atomic nitrogen was of about 1-7% of the N_2-beam equivalent pressure.

The second approach is characterized by the introduction of additional gas species besides the main components, into the growth process, and therefore, belongs to the chemical deposition methods, like metal-organic(MO) -MBE, or gas-source (GS)-MBE. It should be pointed out that high quality c-GaN layers on GaAs substrates have been grown by GS-MBE using DMHy as nitrogen source already in 1991 [4].

2.2. Nucleation

It is widely accepted that nucleation is the most critical step for obtaining c- GaN layers of high phase purity. If the nucleation layer is formed predominantly in the wurzite phase it cannot be transformed into the zinc-blende polytype. Due to the lower total energy of the hexagonal phase compared to the cubic phase a structural transformation of the nucleation layer by any activation steps can be made from the cubic to the hexagonal phase but never vice versa. Wu *et al.* [43] have found in MOCVD experiments that GaN nucleation layers grown at 600°C on (0001) sapphire substrates consist mainly of cubic phase material, which can be transformed into a hexagonal phase after annealing at 950°C. It is obvious from this result that low substrate temperatures are preferable for the formation of the cubic phase of GaN. Therefore, the stabilisation of the cubic phase, which is an indispensable requirement during the nucleation stage, can be supported by a low temperature process. However, since low substrate temperatures generally result in poor crystalline quality, another set of optimized parameters has to be found for the subsequent layer growth. Consequently, the dependence of the structural quality of the c-GaN layers on the nucleation stage is quite complex, if one considers the inherent difficulties of growing metastable phases, which tend to form hexagonal microfacets and inclusions.

According to the growth theory [44] the island-density distribution function and the island-size distribution function have to be measured to analyse the nucleation kinetics of c-GaN. The nucleation of c-GaN on 3C-SiC was investigated by Headrick *et al.* [45] for using real-time x-ray scattering measurements and electron microscopy. Analysing the time dependence of the volume of a growing nucleus and assuming that there is only one characteristic size in the scaling problem, the authors have extracted a value of

m = 2 for the kinetic exponent in the relation

$$V_{cluster} \propto t^{m} \tag{1}$$

where $V_{cluster}$ ist the cluster volume, t the growth time and m a kinetic exponent.

Besides others, the kinetic exponent m contains informations about the island dimensionality. It was concluded that GaN islands initially grow in a quasi-two-dimensional growth mode on 3C-SiC, where the lateral growth velocity is about ten times larger than the vertical growth velocity during the pre-coalescence stage. After coalescence the vertical growth continues at a lower and constant rate. These MO-MBE experiments were performed at a substrate temperature of about 600°C using triethylgallium and ammonia as gas sources.

Similar kinetic studies for the nucleation of c-GaN on GaAs substrates were not reported up to now. However, from the analysis of cross sectional HRTEM images at the c-GaN/GaAs interface a rather detailed qualitative picture of the nucleation process and the defect structure was developed [31]. Accordingly, the nucleation occurs by the formation of three-dimensional islands which are epitaxially oriented with respect to the GaAs substrate. Already in a very early pre-coalescence stage of the nucleation, the islands are plastically relaxed by the formation of edge type misfit dislocations without any climb or glide mechanism. Consequently, the interface between the 3D-islands and the underlying GaAs appears highly distorted. From the existence of regular arrays of edge-type misfit dislocations at the interface, Trampert *et al.* [31] concluded that a coincidence boundary is formed, which is characterized by an array of edge dislocations with a period of five GaN lattice planes. Instead of the macroscopic lattice mismatch of about 20%, a corresponding coincidence lattice mismatch of only -0,02% is effective and therefore, the epitaxial relationship (001)GaAs//(001)GaN, [110]GaAs//[110]GaN obtained reproducibly in the MBE experiments becomes understandable.

Once formed, the isolated 3D-islands of c-GaN on GaAs grow predominantly laterally. When the coalesccence is reached, planar defects like stacking faults and microtwins of high density (10^{10} cm^{-2}) are generated, which extend into the nucleation layer.

In Fig. 2 a High Resolution Transmission Electron Microscopy (HRTEM) image of the c-GaN/GaAs interface region is depicted. It shows a typical c-GaN/GaAs interface, which appears as source for extended planar defects like stacking faults and microtwins. The c-GaN nucleation layer is nearly relaxed just above the interface though there are many stacking faults at the interface. Characteristic pyramid-like structures with {111} facets, which are penetrating from the interface into the GaN layer, can be observed.

In comparison with the defect formation and defect density in c-GaN nucleation layers grown on 3C-SiC substrates some remarkable differences are observed [46]: (i) Due to the smaller mismatch of about 3.7% in the GaN-SiC system, the lattice discontinuity was observed every 30-40 atomic layers, and the defect density at the interface is comparatively smaller than that of the GaN-GaAs interface. (ii) The most outstanding difference is regarded to the flatness of the interface. The interface between c-GaN and SiC is extremly flat, so that even monolayer-step structures can be seen in cross-section HRTEM images. (iii) An additional influence on the formation of cubic islands and nucleation layers undoubtedly results from the presence of As during the nucleation process, as it was proven by nitridation studies [14]. Nitridation is the process

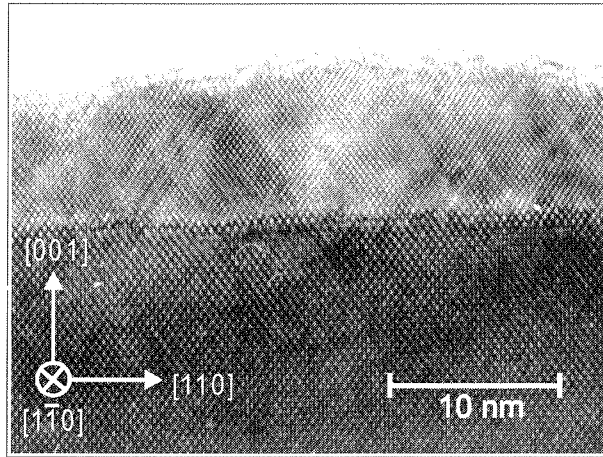

Figure 2. Cross-section high resolution Transmission Electron Microscopy image of the GaN-GaAs(001) interface taken along the [110] direction after deposition of about 20 monolayers (ML) GaN.

to generate a thin GaN layer by exposing the stationary GaAs surface to an nitrogen flux. In this process, As-surface atoms will be replaced by N-atoms due to the stronger Ga-N than Ga-As bond. However, the nitridation of the surface is not initiated uniformly but occurs in a islands like growth mode, as it was found by Okumura *et al.* [46]. At low island density, surface portions which are not covered by the GaN islands tends to react with adatoms, which can generate macroscopic irregularities at the interface. Such irregularities were studied systematically by Lima *et al.* [27], who have demonstrated the additional influence of the surface stoichiometry during the growth of the nucleation layer on the formation of rectangular holes of micrometer size. It should be pointed out that surface irregularities of this type were not reported at interfaces of c-GaN grown on 3C-SiC substrates.

The nucleation stage of the epitaxial growth of c-GaN on Si was investigated by Yang *et al.* [32]. They found that the nucleation of c-GaN directly on (001)Si substrates is obstacled by the formation of amorphous Si_xN_y clusters in the interface region. Due to the low density of GaN-islands, the Si surface atoms can react with N-adatoms forming clusters which leads to phase-mixtured and a textured microstructure of c-GaN layers grown on (001) Si surfaces.

From these results, together with the observations during the nitridation of GaAs surfaces, one can resume that a high island density during the nucleation stage favours the phase purity of the c-GaN. The stabilisation of the cubic phase during the nucleation period is promoted by (i) low substrate temperatures, (ii) a high nucleation density, which minimizes the interaction between the substrate surface atoms and the adatoms involved, in particular the N- adatoms, (iii) the presence of arsenic adatoms.

A high nucleation density is reached at high supersaturation conditions, which implies the use of low substrate temperatures. The requirements (i) and (ii) unavoidable lead to a decrease in the crystalline quality during the nucleation stage. However, by an

intentional insertion of As-adatoms in the nucleation process, as it was proposed by Okumura *et al.* [25], the nucleation temperature and the subsequent grow temperature may be increased without destabilising the formation of the single phase cubic GaN.

It has been mentioned already that the dependence of the structural quality of the c-GaN layers on the nucleation stage is rather complex and obviously of more indirect character. An example for the optimisation of the nucleation process with respect to the resulting structural quality of c-GaN layers is given in the following.

Figure 3 illustrates the dependence of the crystalline perfection of 600-nm-thick GaN layers, which were grown under constant optimum growth conditions on top of 4.5-nm-thick nucleation layers. During the nucleation stage, which was performed always at 600°C, the Ga-flux was the only parameter varied in the experiments. When the atomic N/Ga-flux ratio during the nucleation stage is of about two, the overall crystalline perfection reaches a maximum, expressed as minimum of the corresponding rocking curve width. Obviously, a slight Nitrogen- excess is required during the nucleation process and promotes the formation of cubic islands. As will be seen below, the optimum layer growth conditions of c-GaN, to the contrary, require a slight-Ga excess. Similar results were obtained by Brandt *et al.* [20].

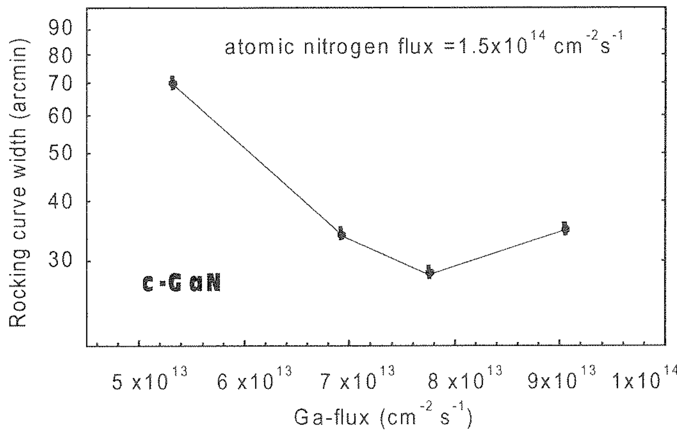

Figure 3. Rocking curve width of the (002) reflection of 600-nm-thick c-GaN layers as a function of on the Ga-flux during the nucleation stage. The atomic N-flux of about N=1.5x 10^{14} atoms/ $cm^{-2}s^{-1}$ was kept constant.

2.3. Growth optimization

The optimum conditions for the epitaxial growth of c-GaN are mainly determined by two parameters, the surface stoichiometry and the substrate temperature. Both parameters are interrelated, therefore an in-situ control of both substrate temperature and surface stoichiometry is highly desirable. It can be achieved by monitoring the MBE growth process by Reflection High Energy Electron Diffraction (RHEED). Surface reconstructions yield evidence for flat and well defined growth surfaces. The study of the surface reconstruction behaviour of c-GaN was one of the key issues for the understanding of the nitride growth and the improvement of the crystalline quality of the

epilayers. Reconstructed (2x2) RHEED patterns of GaN (001) surfaces grown on GaAs were first reported by Strite *et al.* [3]. Powell *et al.* [11] reported a (1x4) reconstruction of GaN (001) surfaces on MgO. Okumura *et al.* [46] also observed a (1x4) reconstruction of c-GaN grown on 3C-SiC. Brandt *et al.* [20] reported transitions between (1x1), (2x2) and c(2x2) surface reconstructions of c-GaN on GaAs. Schikora *et al.* [26] first reported a surface reconstruction diagram for the growth of c-GaN on GaAs. Depending on temperature and the N/Ga flux ratio transitions between (1x1), (2x2) and c(2x2) reconstructions were observed. A similar behaviour was reported by Okumura *et al.* [46]. They find a flux ratio depending transition between a (1x1) unreconstructed (001) GaN surface and a (4x1) reconstruction for the growth on 3C-SiC.

Basically the surface reconstruction is correlated only to the adsorption of adatoms involved. It is well established that the boundaries between different surface reconstructions coincide with iso-adatom coverage contours [47]. Therefore it was surprising that fundamental different surface reconstructions were found experimentally for the same material and surface orientations.

Figure 4 shows the surface reconstruction of c-GaN (001) in dependence of the growth temperature and the Ga-flux at fixed atomic Nitrogen-flow rate. The dots represent the stability range of the c(2x2) reconstruction, the squares show the stability range of the (2x2) reconstruction. A superposition of both reconstructions occurs in a narrow range in between. In Fig. 4 the nominal Ga-flux is related to the flux of atomic nitrogen, which was kept constant in the experiments. Within the whole substrate temperature range, the two distinctly different reconstructions were found to be stable, in accordance with other published results [20]. Under Ga-rich conditions, a c(2x2) reconstruction appears; layers grown under these conditions show n-type conductivity in Hall measurements. The (2x2) reconstruction is associated with N-rich conditions giving rise to p-type conduction [48]. Further increase of the N-excess leads to an unreconstructed (1x1) surface structure. In a narrow range between the c(2x2) and (2x2) regime, both reconstructions occur simultaneously with different intensities of the reconstruction lines, indicating a nearly stoichiometric balance between the atomic N species and Ga adatoms on the surface. All points of the transition curve in the reconstruction diagram coincide exactly with the transition region illustrated in Fig. 1 by the dashed line. This proofs unambiguously that the c(2x2) to (2x2) surface reconstruction transitions are due to a qualitative change of the surface stoichiometry.

The surface reconstruction diagram determined by Okumura *et al.* [46] for (001)GaN on 3C-SiC is depicted in Fig. 5. The Ga-flux is plotted versus the substrate temperature for a fixed N_2-flow rate. The most important difference to Fig. 4 is that the transition curve separates a (1x1) and a (1x4) reconstruction. The (1x1) reconstruction represents Ga-excess whereas the (1x4) reconstruction appears for N-excess conditions. Additionally it was proven that growth conditions on the transition curve yield identical growth rates, indicating the stoichiometric character of the surface. The origin of different reconstructions of GaN (001) surfaces was investigated experimentally by Feuillet *et al.* [24].

They found that the intrinsic reconstructions of GaN (001) surfaces are the (1x1) and the (1x4) reconstructions. The authors exposed the N-rich (1x4) surface, as obtained during growth on 3C-SiC, to an As background pressure of about 10^{-8} Torr. Under As exposure the reconstruction changed from (1x4) to (2x2). For Ga-rich growth conditions the initial (1x1) reconstruction was transformed to a c(2x2) reconstruction under As

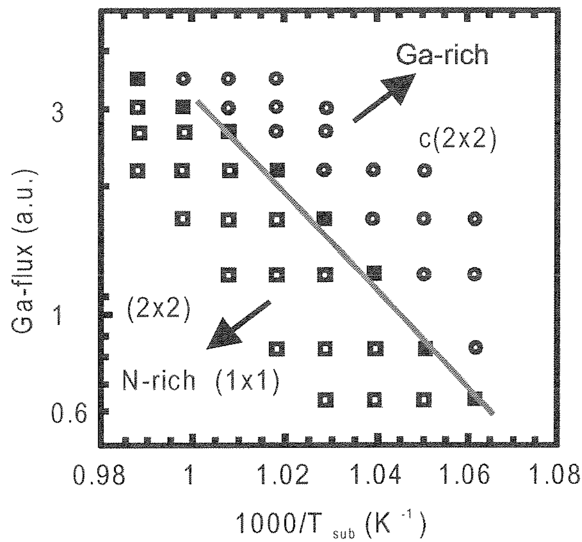

Figure 4. The reconstruction of a c-GaN(001) surface in dependence of the growth temperature and the Ga- flux at fixed atomic Nitrogen-flow rate. The dots represent the stability range of the Ga-rich c(2x2) reconstruction, the squares show the stability range of the N-rich (2x2) reconstruction. A superposition of both reconstructions occurs in a narrow range in between.

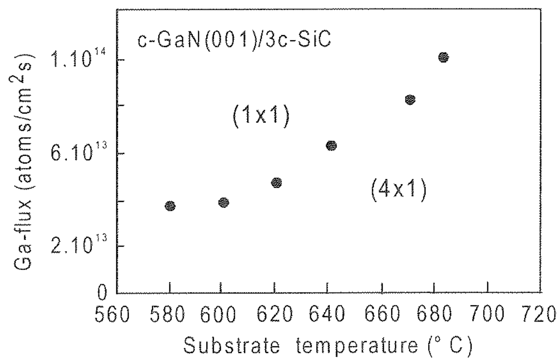

Figure 5. The surface reconstruction diagram of (001)GaN grown on 3C-SiC after Okumura *et al.* [46].

exposure. The remarkable result found in this study was the persistent behaviour observed for the As- mediated surface reconstructions. It was impossible to reverse the As-induced (2x2) and c(2x2) reconstructions back to the corresponding (4x1) and (1x1) reconstructions by decreasing the As cell temperature or increasing the substrate temperature. This result was the first hint that As adatoms, which are intentionally or unintentionally present in the growth process of c-GaN, can act as surfactants stabilizing the cubic structure of the growing surface. Comprehensive and detailed first principle

total energy calculations by Neugebauer *et al.* [49] explained the divergent experimental results. It was found that all energetically favored surfaces modifications of the polar (001) GaN surface are Ga-stabilized and of metallic character. Even under extreme N-rich conditions a Ga-terminated surface is energetically most farorable. Because of the very different cohesive energies of the bulk phases of Ga and N and the small radius of the N atoms, the Ga atoms at the surface can form metallic bonds even without any relaxation similar to those in bulk Ga. They drive the formation of Ga-terminated surface structures in the cubic nitrides. The unreconstructed (1x1) surface obtained experimentally on 3C-SiC substrates under Ga-excess growth conditions as well as on GaAs-substrates under N-excess growth is therefore always Ga-terminated.

For As-free growth the equilibrium surface is a (1x4) reconstructed surface, consisting of linear Ga-tetramers lining up along the [110] direction. The (1x4) surface is energetically only slightly more favourable than the ideal (1x1) Ga-terminated GaN surface. Therefore the (1x4) reconstruction is an intrinsic reconstruction of the polar GaN surface as it was suggested by Feuillet *et al.* [24].

For an environment, where As atoms are intentionally or unintentionally introduced in the growth process, the energetic conditions are drastically changed. The chemisorption of As atoms at the surface significantly reduces the surface energy. Under these conditions a (2x2) structure with a half monolayer coverage of As dimers on a Ga-terminated surface is the most stable configuration. The total energy of this surface is much smaller than the energy of the intrinsic (1x4) reconstruction in the whole thermodynamically allowed range. This explains the experimental result that an As contaminated (2x2) surface cannot be transformed back to a (1x4) reconstruction. In addition the theoretical calculations have shown that structures with As in the second or deeper surface layers are energetically less favorable than structures where As stays in the top surface layer. Therefore As acts as surfactant, which reduces strongly the surface energy and which is virtually immiscible with GaN. The (2x2) and c(2x2) reconstructed surfaces obtained in As-contaminated systems are non-intrinsic surface reconstructions of the (001) GaN surface.

For the growth optimisation some important consequences can be derived [49]. For clean or As-covered c-GaN the surface energy is reduced going from N-rich conditions towards Ga-rich conditions. The stability of the (001) surface decreases and therefore the tendency of forming wurzite clusters increases for N-rich growth conditions. The optimum growth conditions are expected under slight Ga-rich conditions where the surface energy is low.

Independent of the various types of surface reconstructions of the (001) GaN surface, the transition between the Ga-rich and N-rich existence regions is of decisive importance for the experimental control of the growth process. As mentioned above, a prerequisite for the epitaxial growth of high quality c-GaN layers is the maintenance of slightly Ga-rich conditions at a given substrate temperature during the layer growth process. By monitoring the RHEED-intensities of the half-order streaks, which are correlated with the surface composition, growth control can be performed as reported first by Yang *et al.* [30]. The desorption of Ga-adatoms from the (001) GaN surface during short growth interruptions was measured. Due to the desorption of Ga atoms, the surface composition is changed, leading to a variation of intensities of the corresponding RHEED reconstruction lines. In order to quantify the relations, it was assumed that the maximum intensity of the (2x2) reconstruction line in the [-110] azimuth corresponds to

a half monolayer coverage of Ga. Each deviation from this coverage, either by increase of the surface Ga-coverage with subsequent formation of a c(2x2) reconstruction or by increase of the Nitrogen excess, accompanied by the formation of the Ga-terminated (1x1) surface will reduce the maximum intensity of the RHEED reconstruction line. Therefore deviations from surface stoichiometry can easily be estimated *in-situ* from the intensity of the half order reconstruction streak relative to its maximum.

A similar approach where the delay-time of the Ga-desorption during a growth interruption was used as a measure of the deviation from stoichiometric surface conditions is illustrated in Fig. 6. [50] The increase of reconstruction streak intensity after closing the substrate shutter is delayed by a time t_d indicating that during this time the amount of Ga-atoms on the surface exceeds that necessary for the c(2x2) reconstructed surface. Obviously the delay indicates that during t_d a "reservoir" of excess Ga at the surface is emptied keeping the Ga-coverage high. As can also be seen in Fig. 6 t_d measured after a growth period (shutter open) of 4 min is equal to twice the value of t_d obtained after 2 min growth. Therefore t_d reflects the desorption of excess (physisorbed) Ga which is accumulated at the surface. In conclusion, the shorter the delay time t_d, the closer is the surface to its ideal stoichiometric composition.

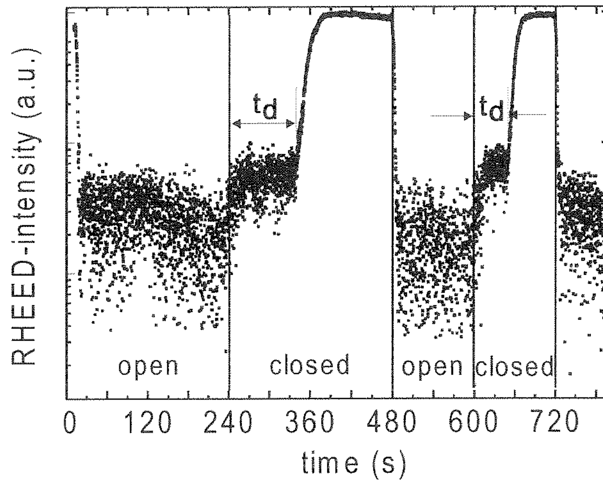

Figure 6. RHEED-intensity of the half-order streak in the [-110] azimuth of a c-GaN (001) surface. The growth interruption and growth continuation is initiated by closing and opening the substrate shutter.

As predicted by the total energy calculations [49] epitaxial growth under N-rich conditions destabilizes the cubic phase and results in the formation of the wurzite phase. The RHEED pattern in Fig. 7 illustrates this behaviour. Integral order streaks of c-GaN and the reconstruction lines at (0,-3/2) are clearly visible as it can be expected for the (2x2) surface reconstruction. Besides this, additional reflections appear in the pattern, which are associated with the formation of microfacets of a wurzite phase as it was concluded from numerical calculations of the RHEED pattern within a kinematic model [26].

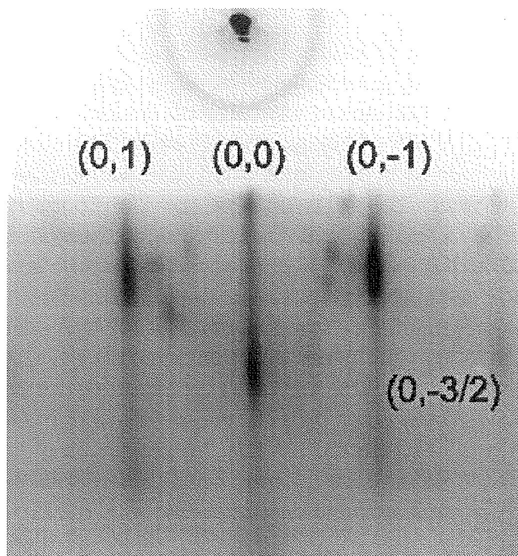

Figure 7. RHEED pattern along the [110] azimuth from a GaN (001) surface at N-rich growth conditions and 720°C substrate temperature.

In contrast to that excess Ga-coverages of the surface favor the formation of Ga-droplets, which are detrimental to the epilayer surface morphology. During growth these Ga-droplets on the surface become saturated by nitrogen and GaN-microcrystals of some μm-size are formed by solution growth. Figure 8 shows a SEM photograph of such a GaN microcrystal with zinc-blende morphology. The crystalline quality of the c-GaN microcrystals is quite high, the PL intensity of the exciton line at 3.27 eV exceeds the intensity of the D/A- recombination line at 3.15 eV by a factor of two, which was not observed with MBE grown c-GaN epilayers up to now.

A powerful tool for the control and optimisation of epitaxial growth are RHEED oscillations, which allow the in-situ control of the growth rate, the layer thickness and the alloy composition with ultimate accuracy. It is generally accepted that RHEED oscillations can only be observed when the growing surface is flat and the growth occurs in a layer-by-layer growth mode. The 2-dimensional layer growth mode on the other hand requires sufficient mobility of the surface adatoms. Zywietz *et al.* [51] investigated the diffusion of adatoms on the surface of nitrides employing density-functional theory. They found that Ga adatoms - their diffusion barrier is about 0.2 eV - are very mobile at typical growth temperatures while the diffusion of N adatoms -the diffusion barrier is about 1.5 eV - is slower by several order of magnitudes. Further calculations have shown that excess N strongly reduces the mobility of Ga-adatoms, due to the formation of strong Ga-N bonds, which have to be broken during the adatom migration.

For these reasons RHEED oscillations are hardly to detect during the growth of c-GaN and are not used routinely for MBE growth control. Nevertheless, RHEED oscillations were first reported by Schikora *et al.* [26] for the MBE growth of c-GaN on GaAs. The RHEED oscillations shown in Fig. 9(a) appear after growth interruption and

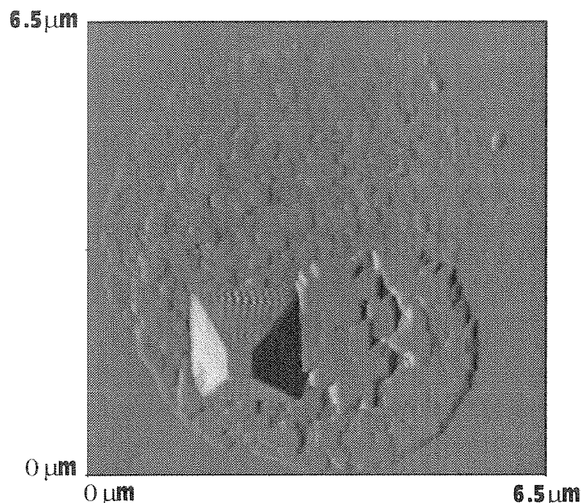

Figure 8. GaN microcrystal with well developed zinc-blende morphology, grown within a Ga-droplet by liquid-solid phase transition.

formation of an N-rich (2x2) surface at a substrate temperature of 740°C. The steep initial rise of the 00-reflection intensity suggests that the growth onset is accompanied by an effective surface smoothing. The oscillations are rapidly damped and entirely disappear when the 00-intensity is recovered to its steady-state level. A growth rate of about 0.08 ML/s was deduced from the oscillation period, which agrees exactly with the growth rate derived from layer thickness measurements by optical interference spectroscopy. The growth oscillations of Fig. 9(b) were recorded under the same growth conditions, however, the surface was exposed additionally to an In-flux of about 10^{-7} Torr beam equivalent pressure. At a substrate temperature of 740°C one can assume that practically no In-incorporation occurs and therefore, In most probably acts as surfactant. It is evident from Fig. 9(b) that the growth oscillation are much more pronounced and the oscillation period is changed suggesting an increased adatom mobility when In-adatoms are involved in the surface kinetics. This conclusion was supported recently by theoretical studies of surfactants for GaN-growth [52]. These calculations revealed that due to the presence of In on the surface, a second diffusion channel for the N adatoms is established, which reduces the diffusion barrier for N-adatoms by sub-surface diffusion. As a consequence, the mobility of N-adatoms increases and the 2-dimensional layer by layer growth mode is stabilized. However, In adatoms also influence the Ga- adatom kinetics and the resulting growth rate, as confirmed recently by Adelmann *et al.* [53]. There is no doubt that further investigations of the role of different surfactant atoms, like As, In, Bi or Sb are necessary and helpful to improve the MBE of c-GaN. It should be noted that growth oscillations can be measured easier for h-GaN MBE and were used for the control of the alloy composition of InGaN-alloys [22].

In spite of the difficulties inherent to the c-GaN MBE growth an impressive demonstration of the high level of growth control reached so far up to now was given recently by Martinez-Guerrero *et al.* [23]. The authors reported the first self-assembled

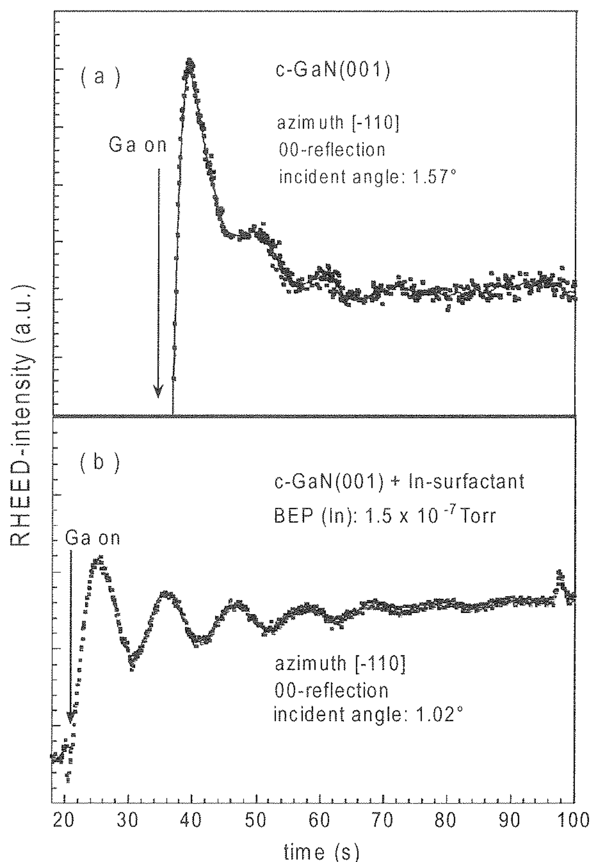

Figure 9. RHEED-oscillations of the 00-reflection in the [-110] azimuth. Curve (a) shows the growth oscillations under normal growth conditions, curve (b) shows the growth oscillations with In-adatoms added to the surface.

growth of stacked c-GaN quantum dots QDs) using the Stranski-Krastanow growth mode. The GaN quantum dots (QD) were formed on AlN buffer layers, which were grown on 3C-SiC substrates. A basic prerequisite for the Stranski-Krastanow transition is the existence of a flat, 2-dimensional wetting layer, which is elastically strained. For the growth of stacked QDs, the overgrowth of the 3-dimensional islands by the barrier layer material must be optimized. The 2-dimensional surface has to be recovered rapidly for the following Stranski-Krastanow transformation. Using RHEED-control, atomic force microscopy and transmission electron microscopy it was demonstrated that these requirements were met in the MBE-experiments resulting in GaN islands densities of about 10^{11} cm^{-2} [23]. The embedded c-GaN QD showed strong ultraviolet photoluminescence without any thermal quenching up to room temperature. Due to the fact that coherent growth of self-assembled QD exhibits particular advantages when the surrounding crystal matrix disposes a large number of defects, as it is the case in the

group III nitrides, it can be expected that these quantum dot structures will open new fields of applications of the cubic nitrides.

3. Doping of cubic GaN

For advanced optoelectronic devices, like light emitting diodes (LEDs), or laser diodes (LDs) controlled p- and n-type doping is crucial. [54,55] Dopants are intentionally introduced to control the type and the magnitude of the electrical conductivity. The dopants are chosen for optimum device performance. Therefore, the development of any semiconductor device technology requires the selection and characterization of dopant impurities. The research of c-III-nitrides is currently at this stage.

Up to now, Silicon and Magnesium were used as standard donor and acceptor dopants in MBE. However, Magnesium has several disadvantages, which limit the doping efficiency of Mg in GaN to maximum hole concentrations in the upper 10^{17} cm^{-3} range. This is mainly ascribed to large acceptor ionization energy and compensation effects [56]. Experiments showed that Mg is volatile, requires low substrate temperatures and N-rich growth conditions [57,58]. These conditions are disadvantageous for the epitaxy of high quality c-GaN layers, since N-rich conditions deteriorate phase purity [26].

Among possible alternative acceptor dopants especially Carbon has received a considerable interest due to its similarity to nitrogen in atomic radius and electronegativity. Carbon doping of hexagonal Gallium Nitride (h-GaN) led to semi-insulating properties or to a reduction of background electron concentration [59-61]. Abernathy *et al.* [62] reported on p-type doping of c-GaN by carbon. However, due to the use of CCl_4 a pronounced reduction in growth rate prohibited the incorporation of higher C concentrations and the maximum hole concentration reached was $3x10^{17}$ cm^{-3}.

3.1. N-type doping

Elements of the group IV on group III-site and elements of the group VI on N-site can be incorporated as donors for n-type doping of group III-nitrides. The group-VI impurities include O, S, Se and Te. Considering the atomic radius only O fits the N-atom size and is believed to be incorporated easily. The group-IV impurities include C, Si, Ge, Sn and Pb. The latter element has a large atomic radius and is therefore not expected to incorporate easily in III-Nitride semiconductors. The remaining group-IV impurities, i.e. C, Si, Ge, and Sn share different charcteristics. First, all column IV impurities are amphoteric, i.e. they can occupy either the group-III or the nitrogen site of the zinc-blende lattice. As a result, group-IV impurities are donors or acceptors for cation site or anion site, respectively. Second, due to their amphoteric nature column-IV impurities may autocompensate and the electrical activity may saturate at high impurity concentration. However, C has a size comparable to the N-atoms and is therefore expected to be mainly incorporated as an acceptor. Si, Ge and Sn are expected to replace Ga-atoms and act as a donor. These considerations show that Si and O may be the most appropriated elements for n-type doping of GaN.

Doping of MBE grown c-GaN by Si was reported by As *et al.* [63], Martinez-Guerrero [64] and Li *et al.* [65]. Elemental Si was evaporated from an effusion cell at source temperatures between 750°C and 1200°C.

In Fig. 10 the Si-concentration measured by SIMS (full squares) and the free electron concentration measured by Hall-effect at room temperature (full triangles) are shown as a function of the Si source temperature T_{Si}. Both the amount of incorporated Si as well as the free electron concentration follows exactly the Si-vapor pressure curve (full line in Fig. 10) at T_{Si}>1000°C [66]. The agreement between the values measured by Hall effect and SIMS implies that all Si atoms are incorporated at Ga sites and act as shallow donors. The maximum free electron concentration and mobility achieved so far are $5x10^{19}$ cm^{-3} and 75 cm^2/Vs at room temperature, respectively. The concentration and depth distribution of Si were measured by secondary ion mass spectroscopy (SIMS) using implanted calibrated standards for quantification, and an O^{2+} primary beam of 6 keV. Figure 11 shows the depth profile of Si, GaN and As for a c-GaN epilayer doped with elemental Si at a Si-flux of $5.7x10^{11}$ $cm^{-2}s^{-1}$. Silicon is homogeneously distributed and no accumulation, neither at the interface nor at the surface was observed. At a depth of 0.4 μm the Si-concentration was measured to be $2x10^{19}$ cm^{-3}. This demonstrates the ability of Si to be incorporated in a controlled way for n-type doping of cubic GaN up to concentrations, which are necessary for the fabrication of optoelectronic devices.

At room temperature the optical properties are strongly related to the Si-doping level. The integrated intensity of the luminescence (full dots in Fig. 10) followed the Si-vapor pressure curve and even at the highest free carrier concentration of $5x10^{19}$ cm^{-3} no

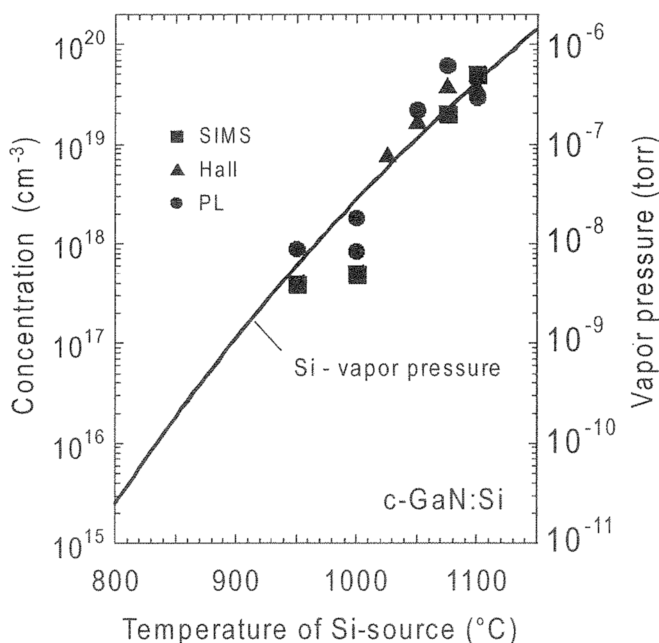

Figure 10. Free electron concentration in Si-doped c-GaN measured by Hall-effect (full triangles), Si concentration measured by SIMS (full squares), and integrated room temperature PL intensity (full circles) versus Si effusion cell temperature. The full curve represents the vapor pressure of Si [66].

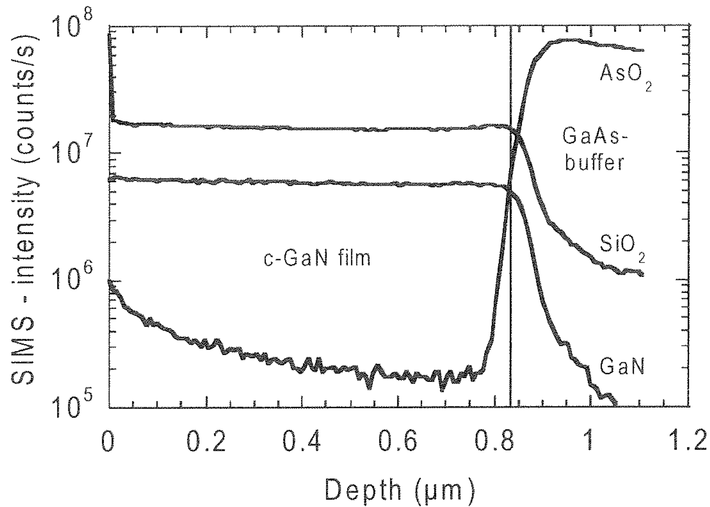

Figure 11. SIMS depth profiles of a Si doped cubic GaN epilayer on a GaAs (001) substrate (Si-flux: $5.7x10^{11}cm^{-2}s^{-1}$).

quenching of the luminescence was observed. The optical properties of Si doped cubic GaN at low temperature are depicted in Fig. 12. At 2 K the spectrum of the sample grown with the lowest Si-flux ($8.5x10^{5}$ $cm^{-2}s^{-1}$, T_{Si} =750°C) is dominated by the excitonic transition X at 3.26 eV and by the donor-acceptor pair transition (D°,A°) at 3.15 eV [67]. The binding energies of the donor and acceptor involved in the (D°,A°) pair recombination were estimated to be 25 meV and 130 meV, respectively. A clear shift of the (D°, A°) emission to higher energies was observed with increasing Si flux.

Beyond a Si-flux > $1.2x10^{11}$ $cm^{-2}s^{-1}$ the (D°,A°) transition and the excitonic transition merge to one broad band and the peak maximum shifts monotonically towards higher energies with increasing Si doping. At the same time the spectral lineshape of the main emission becomes strongly asymmetric with a steep slope on the high-energy side and a smooth slope on the low energy side of the spectrum. Such a behavior is characteristic for momentum nonconserving (nonvertical) band-to-band transitions or to recombination of free electrons to local hole states and has been observed in the spectra of GaAs heavily doped with Te [68] or Si [69]. The high energy edge of the luminescence band was determined by the electron Fermi-level which shifts to higher energies (Burstein-Moss shift [70]) as the conduction band is filled up with free electrons. is indicated by arrows. In the highest doped sample the energy at half maximum intensity $E_{1/2}$ has a value of 3.342 eV. For a corresponding carrier concentration of about $5x10^{19}$ cm^{-3}, however, band filling of 240 meV was calculated using an electron effective mass of 0.2 in GaN [55]. This indicates that due to exchange interaction between free carriers the energy gap of cubic GaN has been shrinked from 3.305 eV without doping to 3.095 eV at an electron concentration of $5x10^{19}$ cm^{-3}. As it is known from GaAs, the reduction in band-gap energy due to the so called band-gap renormalization (BGR) can be described by a n1/3 power law [71]. A BGR coefficient of $-5.7x10^{-8}$ eVcm was obtained for cubic GaN, which is comparable to that of hexagonal

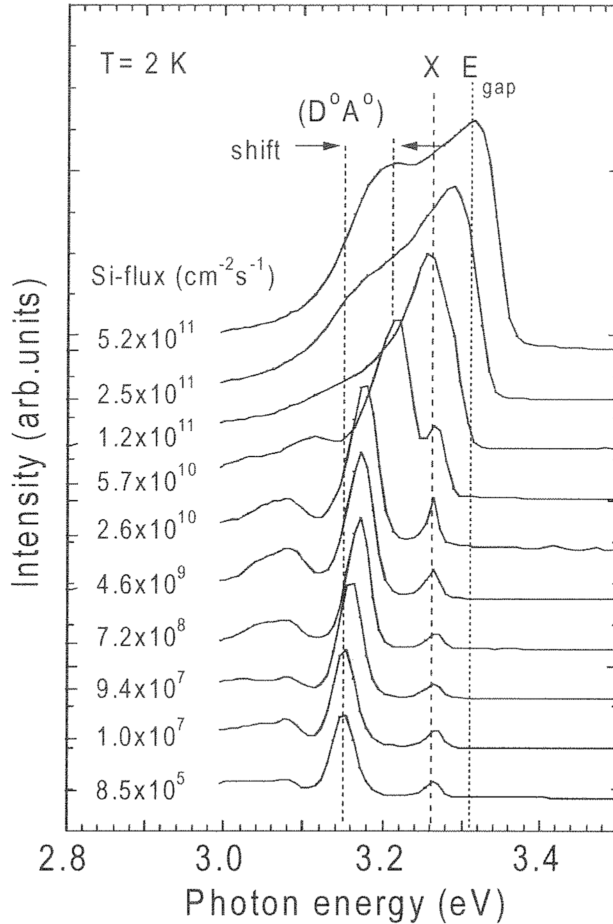

Figure 12. Low temperature PL spectra of Si doped cubic GaN.

GaN (-4.7×10^{-8} eVcm) [72]. A detailed analysis of the band gap narrowing in Si doped cubic GaN has been performed in Ref. 73.

The electrical properties of Si doped c-GaN are depicted in Fig. 13 where $1/q.|R_H|$ is plotted versus the Si-flux. R_H is the Hall constant and q is the electronic charge. At Si-fluxes higher than 3×10^{10} $cm^{-2}s^{-1}$ the samples were n-type (full triangles) and, as already discussed in Fig. 11, the measured free electron concentration exactly followed the Si-flux (dotted line). Temperature dependent Hall-effect measurements further showed that these c-GaN samples were fully degenerated. However, all samples doped with a flux lower than 3×10^{10} $cm^{-2}s^{-1}$ were p-type with a hole concentration of about 2×10^{16} cm^{-3}. The hole concentration was independent of the Si-flux and was equivalent to the hole concentration of nominally undoped c-GaN epilayers [48,74]. Thus it was concluded that a residual acceptor concentration of about $N_A = 4 \times 10^{18}$ cm^{-3} exists in cubic GaN epilayers, and that the Si-donors have to compensate these acceptors.

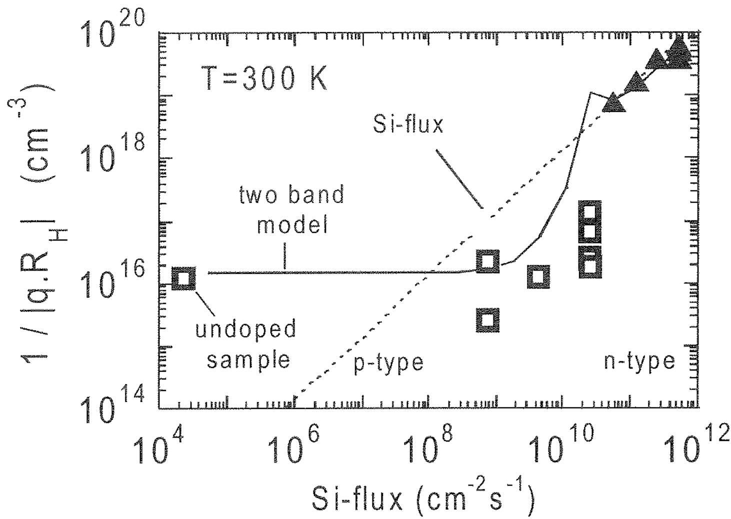

Figure 13. The inverse, room temperature Hall-constant $1/q.|R_H|$ of Si doped c-GaN versus Si flux. R_H is negative above $3x10^{10}$ $cm^{-2}s^{-1}$ and positive below $3x10^{10}$ $cm^{-2}s^{-1}$.

From temperature dependent Hall-effect measurements of nominally undoped c-GaN samples a thermal activation energy of about $E_A \cong 0.166$ eV and acceptor concentrations NA of about $4x10^{18}$ cm^{-3} were estimated [74]. At room temperature the hole concentration was $p = 1x10^{16}$ cm^{-3} and the hole mobility was μ_p =283 cm^2/Vs. This value is included in Fig. 13 by an open square at the left side. The acceptor concentration N_A is in excellent agreement with the value estimated from the p to n transition that occured in the Si-doping experiments. Assuming a constant residual acceptor concentration and taking the room temperature values of the undoped samples for p and μ_p, a simple two-band conduction model [75] was applied to calculate $1/q.|R_H|$ versus Si-flux. The results of the two-band model are depicted in Fig. 13 by the full curve and explain in a reasonable way the experimental observation.

In Fig. 14 the room temperature mobilities (μ_n, μ_p) of Si-doped c-GaN epilayers are plotted versus the measured free carrier concentration (n, p). The full dots and the full triangles represent samples showing n-type conductivity. The open squares correspond to nominally undoped p-type reference samples. The influence of the high dislocation density ($\approx 10^{11} cm^{-2}$) on the electrical properties of c-GaN of layers grown on GaAs is reflected by the dependence of the electron mobility on the free carrier concentration. Similare to hexagonal GaN [76] the mobility first increases with carrier concentration, reaches a maximum value of about 82 cm^2/Vs at an electron concentrations of $3x10^{19}$ cm^{-3} and decreases again. This behavior is characteristic for dislocation scattering and was explained by a theory recently developed for charged-dislocation-line scattering [77]. Theoretical calculations further showed that in c-GaN edge dislocations shall introduce acceptor like states roughly 200 meV above the valence band maximum [78]. This implied that threading edge dislocations are electrically active in cubic GaN.

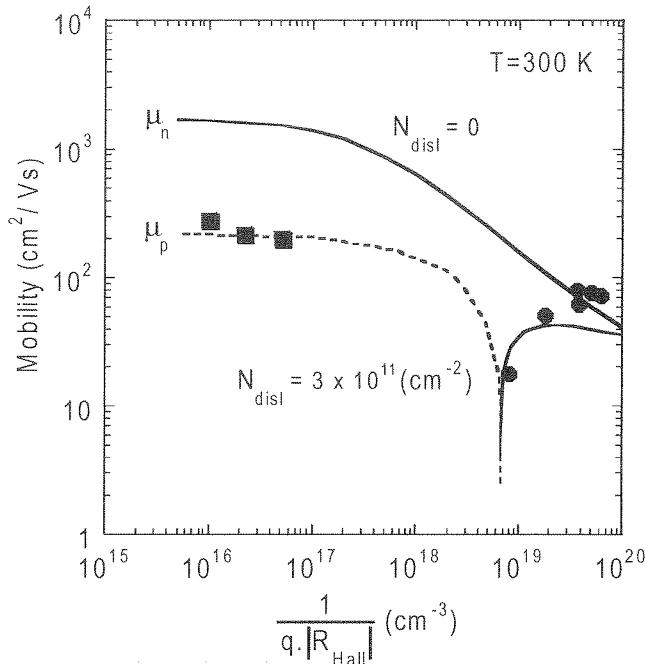

Figure 14. Room temperature mobility of Si-doped c-GaN versus $1/q.|R_H|$. Dots and squares are experimental data, curves are calculated including scattering by dislocations which act as acceptors. Full curve and dots-negative R_H; dashed curve and squares - positive R_H.

X-ray diffraction and Rutherford Backscattering experiments revealed that the dislocation density N_{disl} in c-GaN/GaAs is of the order of 10^{11} cm^{-2} [79,80]. According to Weimann *et al.* [76] a residual acceptor concentration of about $6x10^{18}$ cm^{-3} was estimated. This value agreed with the acceptor concentration necessary to explain the p- to n-type transition.

The curves in Fig. 14 represent calculations of the room temperature mobility versus carrier concentration for different electrically active dislocation densities N_{disl}. For this calculations polar optical phonon scattering, acoustic phonon scattering, ionized impurity scattering and dislocation scattering were taken into account. The full lines are for n-type and the dotted lines for p-type conductivity. The best agreement with experimental results is obtained for a dislocation density of about $3x10^{11}$ cm^{-2} in good agreement with x-ray diffraction data.

3.2. P-type doping

Controlled p-type doping is still a challenge in the growth of group III-nitrides. In GaN the group II, Ga-site acceptors Be, Mg, Ca, Zn and Cd, together with the group IV, N-site acceptor C are potential p-type dopants. A common drawback to all these acceptors is their large activation energy of about 200 meV, which limits the fraction of ionized acceptors at room temperature to about 1%. Therefore, acceptor concentrations in the order of 10^{20} cm^{-3} are needed for hole densities in the mid 10^{18} cm^{-3} range - as they

are typical for e.g. laser diodes. However, such high acceptor concentrations severely reduce the mobility due to scattering at neutral and charged impurities. In addition, the limited solubility of the dopants or the tendency for selfcompensation further prevents high doping concentrations. The great experiences accumulated with hexagonal GaN showed that Mg is the prefered p-type dopant. However, Mg is subjected to several disadvantages like self-compensation, segregation and solubility effects which limit the usually reported doping efficiency of Mg in hexagonal GaN to maximum hole concentrations in the upper 10^{17} cm^{-3} [56]. Doping experiments were less extensively reported in cubic GaN [81-83] and were mostly concentrated on Mg [10,64,84-87]. Results of Be doping were quite disappointing since no p-type conductivity could be achieved [88], however using co-doping of Be and O p-type conduction was demonstrated and resistivites as low as 0.02 Ωcm were measured [82]. A promising new acceptor in c-GaN is C which gave hole concentrations close to 10^{18} cm^{-3} at room temperature [89-92].

Mg doping of cubic GaN has been reported by Lin *et al.* [10], As *et al.* [85] and Martinez-Guerrero *et al.* [64]. Whereas Lin *et al.* injected Mg into the ECR source using N_2 carrier gas to enhance sublimation of Mg atoms, As *et al.* and Martinez-Guerrero *et al.* evaporated Mg from commercial effusion cells. Lin *et al.* obtained p-type c-GaN epilayers on GaAs (001) substrates at low growth temperatures (580°C). Hole concentrations between $8x10^{16}$ and $8x10^{18}$ cm^{-3}, and room temperature hole mobilities between 39 and 4 cm^2/Vs were obtained. Depth profiles of Mg in GaN showed a severe Mg surface segregation. Since Mg was fed through the ECR source, primarily Mg^+ ions were believed to be incident at the growth surface.

Using Mg effusion cells it is expected that neutral Mg is incorporated into the c-GaN epilayers. In Fig. 15 the Mg concentration incorporated in c-GaN at 720°C as measured

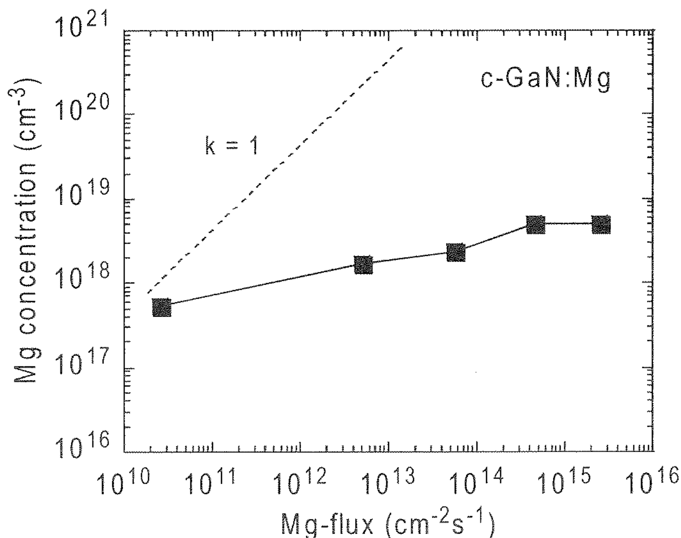

Figure 15. The Mg concentration in c-GaN measured by SIMS (squares) versus flux of the Mg-doping cell. The dashed line corresponds to a Mg-concentration proportional to the flux of Mg atoms.

by SIMS is plotted versus the Mg flux (squares). Assuming a sticking coefficient of 1 for Mg the dashed line is expected. However, although the Mg-flux was varied by more than four orders of magnitude the Mg concentration varied by only one order of magnitude (full line). The Mg doping level remains below $5x10^{18}$ cm^{-3} and seems to saturate at high Mg fluxes. A similar behavior was observed for MBE growth of hexagonal GaN [57] and GaAs [93] and was expected to be due to the high vapor pressure of Mg resulting in a high reevaporization rate of the physisorbed Mg atoms. It was suggested that Mg incorporation occurs either via the presence of a saturated surface layer of Mg or via the presence of specific configurational sites for Mg incorporation, so that the incorporation is nearly independent of the Mg arrival rate [57]. Recently, Mg incorporation as high as $1x10^{20}$ cm^{-3} has been reached at lower growth temperatures (T_{sub}=680°C) for cubic GaN grown on cubic SiC (001) [64]. However, at Mg doping levels exceeding 10^{19} cm^{-3} a severe degradation of the crystalline quality of the cubic GaN layers was observed [87] and unfortunately no correlation between the hole and the Mg concentration has been found.

SIMS depth profiles of Mg in cubic GaN showed two characteristic features at the surface and at the GaN/GaAs interface and a homogeneous Mg distribution in between [85]. At the surface a slight increase of the Mg signal occured, indicating segregation of Mg. At the GaN/GaAs heterojunction an accumulation of the Mg atoms by more than one order of magnitude was observed. This effect was attributed to an increased diffusion of Mg to the GaAs substrate, similar to the observations made in Ref. 58 for h-GaN on sapphire substrates. Due to the low operating temperature of the Mg cell it is not very likely that transient effects of the Mg flux just after opening of the shutter will result in this increased incorporation. However, the increased density of structural defects near the interface due to the large mismatch between substrate and epilayer may cause accumulation of Mg atoms. A significant amount of Mg was also found in the nominally undoped GaN sample grown just after the doping experiments, due to memory effects of the growth chamber.

Hall-effect measurements of the Mg-doped cubic GaN epilayers revealed that the layers were p-type. In contrast to samples grown by metal organic chemical vapor deposition no postgrowth treatment was required for GaN films grown by plasma-assisted molecular beam epitaxy (MBE) since it employed hydrogen-free nitrigen plasma as a source of active nitrogen. Figure 16 shows the temperature dependence of the hole concentration and of the hole mobility (insert) of a sample doped with a Mg-flux of 10^{13} $cm^{-2}s^{-1}$ ($[Mg]_{SIMS}=1.7x10^{18}$ cm^{-3}). Under the assumption of compensation the temperature dependence yields for the shallow Mg acceptor an activiation energy of $E_{Mg}=0.110 \pm 0.020$ eV. [84] The corresponding value for hexagonal GaN is 160 ± 5 meV [94]. However, as shown later in both cases the thermal activation energies are much lower than the optical activation energies, which may be due to a strong relaxation effect of the negatively charged Mg [95].

With increasing Mg flux no increase of the free hole concentration p_{Hall} was observed at room temperature, it was even slightly decreasing with increasing Mg flux (see also Fig. 18). The SIMS measurements, however, showed that the amount of incorporated Mg increased, indicating that an Mg related compensating donor may be incorporated during Mg-doping. This assumption is corroborated by PL-measurements.

Figure 17 shows 2 K photoluminescence spectra of cubic GaN epilayers grown at a substrate temperature of 720°C, which were doped using different Mg fluxes. The lowest

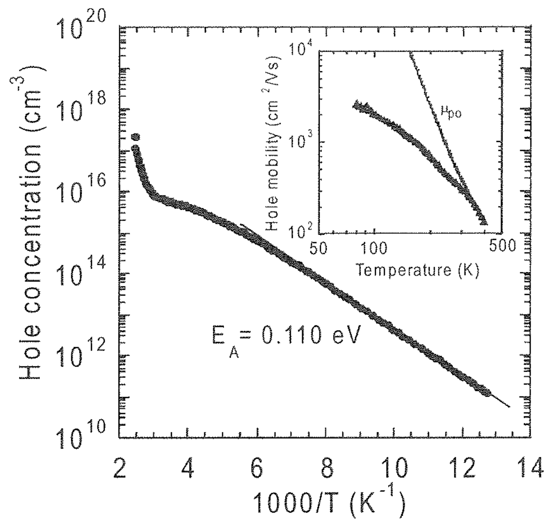

Figure 16. Hole concentration of a Mg doped c-GaN epilayer (Mg-flux 5.7×10^{13} $cm^{-2}s^{-1}$) as a fuction of the inverse temperature. The activation energy of the shallow acceptor level is 0.110 ± 0.020 eV. The inset shows the temperature dependence of the hole mobility, which is dominated by polar optical phonon scattering at temperatures above 300 K (full line).

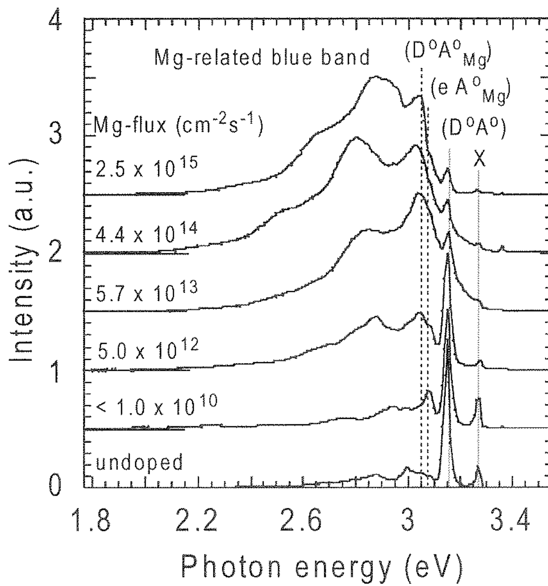

Figure 17. Low temperature (2K) photoluminescence spectra of Mg doped c-GaN layers. The lowest spectrum corresponds to an undoped sample grown before introducing Mg into the MBE growth chamber (excitonic transition X at 3.26 eV and omnipresent donor-acceptor pair transition (D^0,A^0)). The dashed lines indicate Mg-related transitions $(e,A^0{}_{Mg})$, $(D^0,A^0{}_{Mg})$. Below 2.95 eV, a Mg-related blue emission band is observed, which is modulated due to interference effects in the layer.

spectrum is that of an undoped reference sample grown before introducing Mg into the chamber. Mg-doping at fluxes below 10^{13} $cm^{-2}s^{-1}$ results in the appearence of a donor acceptor transition (D^0,A^0_{Mg}) at 3.04 eV. The donor participating in this line has the same ionization energy as the one observed in the undoped sample. From the emission energy an acceptor activation energy of E_{Mg} = 0.229 eV is estimated. This energy is in excellent agreement with recent theoretical calculations of Mg_{Ga} for c-GaN [96] and is somewhat lower than that for the corresponding value of 0.265 eV for h-GaN [97]. At Mg-fluxes exceeding 10^{14} $cm^{-2}s^{-1}$ the low energy side of the spectrum is dominated by a broad blue emission band centered at about 2.85 eV, which is modulateddue to interference effects (upper curves in Fig. 17).

With increasing Mg-flux a clear increase of the integral intensities of the shallow transitions (D^0,A^0_{Mg}) and (e,A^0_{Mg}) as well as the deep "blue" band was measured (see Fig. 18), revealing that all three transitions are directly related to Mg incorporated in c-GaN. Whereas the shallow transitions saturated at higher Mg-flux, this was not observed for the blue emission. Since the free hole concentration was nearly independent of the Mg amount it was concluded that the impurity involved in the blue band acts as a compensating deep donor center [84]. This observation was in agreement with similar observations made in h-GaN [98].

Temperature dependent PL-measurements showed that the binding energies of the shallow Mg related acceptor and the deep Mg-related donor are 0.229 eV and 0.239 eV,

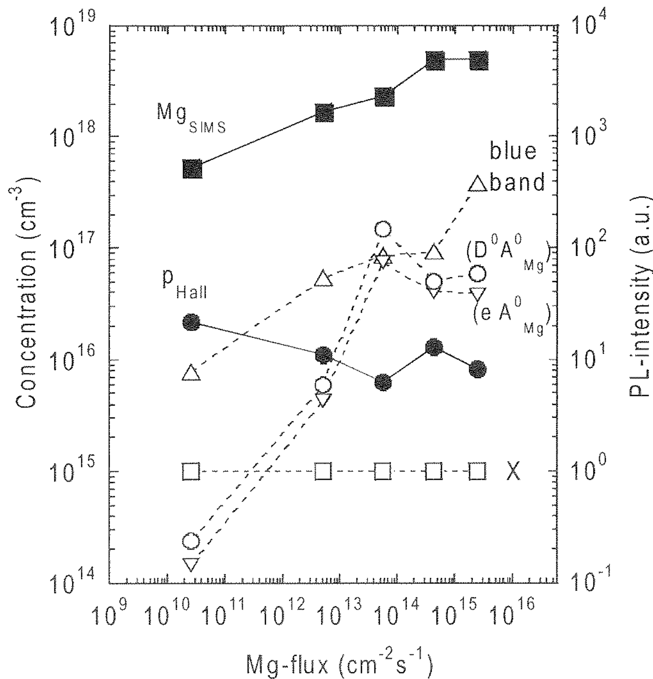

Figure 18. The intensities of Mg-related PL emission lines, the room temperature hole concentration p_{Hall} and the Mg concentration measured by SIMS of Mg-doped c-GaN layers versus flux of the Mg-effusion cell.

respectively. The nature of this deep donor is unknown up to now, however it indicated that also in c-GaN Mg is incorporated at different lattice sites or forms complexes at high Mg fluxes. Theoretical calculations showed that Mg_i, Mg_N or Mg-V_N act as compensating deep donors in GaN. Since the formation energies of all these Mg-related defects are low they are possible candidats for the impurity involved in the blue band emission [96]. In h-GaN this blue band was attribute to Mg-V_N complexes [99].

Rapid thermal annealing experiments (30 s) in N_2 atmosphere showed that the defect related to the blue band is thermally stable up to an annealing temperature of 1100°C. P-type doping by Mg under N-rich growth conditons, which has been shown to be benefitable in Mg-doping of hexagonal GaN [58], resulted in increased hexagonal inclusions in c-GaN.

Due to the successful p-type doping of GaAs with C, it has been suggested that carbon is an acceptor for GaN. Carbon is an acceptor in GaN when substituting nitrogen [100] [101]. Carbon is the only group IV element that has a small enough atomic radius to fit the nitrogen site. Compared with other group II acceptors such as Mg, carbon is much less volatile and therefore not prone to cause memory effects in the MBE growth system. Theoretical calculations reveal that C_N is an effective mass acceptor and that the incorporation of C on the N site is preferred. However, due to the amphoteric nature of C the concentration of C_N and C_{Ga} may be comparable. In addition at high doping concentrations C_{Ga} and C_N have a strong tendency to form C_{Ga}^+-C_N^- nearest neighbour pairs, leading to self compensation [102,103].

A previous study of carbon doping of c-GaN grown by metal organic molecular beam epitaxy (MOMBE) on GaAs substrates indicated that carbon created shallow acceptors and p-type conductivity [62]. However, due to the use of CCl_4 a pronounced reduction in growth rate prohibited the incorporation of higher C concentrations.

No successful p-type doping of hexagonal GaN by carbon has been reported up to now. High-quality semi-insulating C-doped GaN layers with resistivies greater than 10^6 Ωcm have been grown with high reproducibility and reliability using methane gas (cracked by an ion gun) as a carbon source in MBE [104]. Carbon doping using a resistivity heated graphite filament in rf-plasma assisted MBE lead to a reduction of the background electron concentration by one order of magnitude but the material remained n-type [61]. At high carbon concentration a re-increase of the electron concentration was observed, which was attributed to the introduction of a new carbon related donor.

Since carbon is present as a contaminant in most MOCVD processes, its role in the compensation and unintentioned doping of GaN layers may be significant. Huge amounts of carbon ($>2 \times 10^{19}$ cm^{-3}) have been found in h-GaN proven by low-pressure MOCVD using dimethylhydrazine (DMHy) as a group V source [105]. In plasma assisted MOCVD using CH_x as a carbon source SIMS analysis indicated large amounts of C and H ($\sim 10^{19}$ to 10^{20} cm^{-3}) in the samples [106]. After annealing under a nitrogen atmosphere, the films remained highly resistive. It was suggested that the C-H complex is thermally stable and that H may passivate the C acceptors [106]. In HVPE samples it was found that the incorporation of carbon by an propane/H_2 mixture produces a significant yellow luminescence around 2.2 eV [60] similar to the yellow luminescence observed by Ogino *et al.* [107] in intentionally C doped micro crystal powder and needle like crystals. Photoluminescence investigations on undoped n-type GaN layers grown on 6H-SiC and sapphire [108] and on Si [109] reveal the presence of residual acceptors

with an optical binding energy of 230 meV, which is attributed to carbon on nitrogen sites.

Carbon doping of MBE grown c-GaN on GaAs (001) substrates was achieved by e-beam evaporation of a graphite rod through adjusting the applied e-beam power [89]. The C-flux was externally calibrated by means of growing C-doped Gallium Arsenide, assuming a similar sticking coefficient of C on GaAs and GaN. It followed that a maximum C-concentration of about 10^{20} cm^{-3} should be achievable in c-GaN. This was confirmed by SIMS measurements, which indeed showed a C incorporation in c-GaN of $2x10^{20}$ cm^{-3}.

The room temperature hole concentration as a function of the carbon flux of C-doped cubic GaN epilayers is shown in Fig. 20. The hole concentration increased up to a maximum value of about $6x10^{17}$ cm^{-3} at a C-flux of 10^9 $cm^{-2}s^{-1}$. This value was about one order of magnitude higher than the value obtained by Mg-doping of cubic GaN [81] and demonstrates the ability of C for p-type doping of cubic GaN. However, at high C-fluxes a clear reduction of the free hole concentration was observed. This indicates that at high C concentrations additional compensating centres were generated.

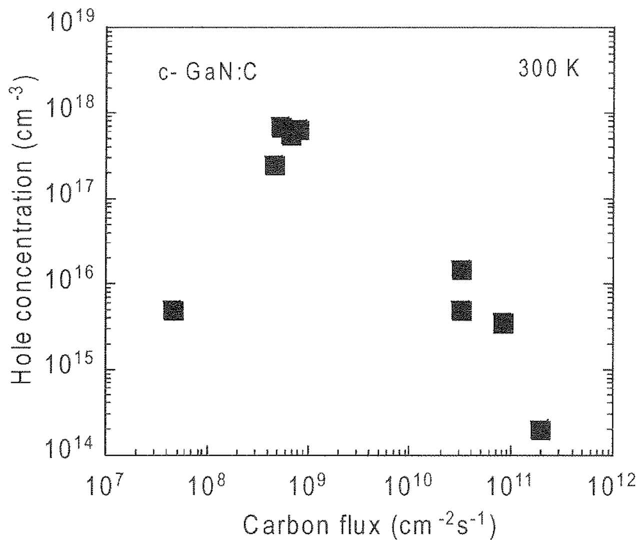

Figure 19. Room temperature hole concentration of C-doped c-GaN versus flux of the Carbon evaporation source.

The incorporation of Carbon in cubic GaN has a profound influence on the PL, as can be seen in Fig. 20. A photoluminescence emission band at E = 3.08 eV appeared in the 2 K spectra of slightly doped c-GaN layers. This transition was clearly different from the well-known line at 3.27 eV (X) and at 3.16 eV (D^0,A^0) [67]. A detailed analysis of the 3.08 eV band showed, that it was a convolution of two distinct lines separated by 25 meV at low temperatures (indicated by arrows in Fig. 20). At temperatures above 100 K the low-energy contribution thermalizes and only the high-energy PL emission was observed. Thus, the lower transition was attributed to a donor-acceptor recombination

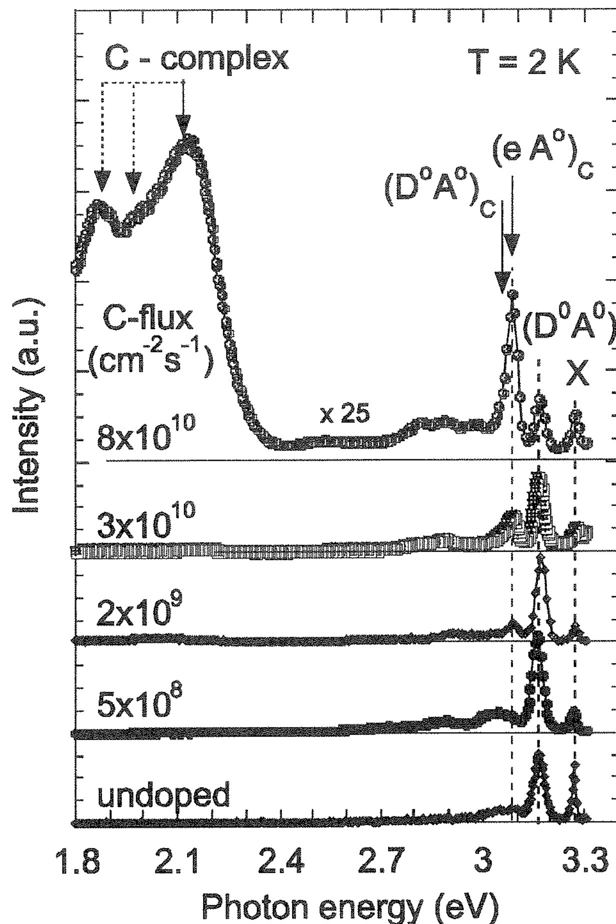

Figure 20. Photoluminescence spectra of c-GaN layers with different Carbon doping levels. The intensity of the topmost spectrum has been multiplied by a factor of 25.

$(D^0,A^0)_C$ and the other to a C-related band-acceptor recombination $(e,A^0)_C$, respectively.

From temperature dependent PL-measurements E_A = 215 meV has been estimated for the binding energies of the shallow C related acceptor. This value is 15 meV below that of the Mg acceptors in c-GaN [85] and is also below the value known for hexagonal GaN:C [108]. The donor involved has the same ionisation energy (25 meV) as the one observed in the undoped and Mg-doped c-GaN samples [67].

At moderate Carbon concentrations the integrated intensity of the 3.08 eV band increased linearly with the Carbon flux [91]. This is in agreement with the assumption that the intensity of a donor-acceptor emission is proportional to the amount of acceptors involved [110]. Above a C-flux of 10^{10} $cm^{-2}s^{-1}$ however, the donor acceptor band intensity decreased sublinearly indicating that at high C-concentrations additional deep compensating centers are introduced which bypass the recombination via shallow carbon

acceptors. This assumtion is supported by the appearance of a red luminescence at 2.1 eV in the topmost spectrum of Fig. 20.

The strong decrease of the carbon related donor-acceptor transition may have two reasons. First at high concentrations C atoms may form complexes, which do not act as acceptors. This would reduce the number of shallow C acceptors involved in the transition and would decrease its intensity. Second the formation of a deep defect either by C-complex formation or by the introduction of deep intrinsic defects may decrease the internal quantum efficiency which quenches the acceptor related PL.

The red luminescence at 2.1 eV is related to localized deep defect states. This was confirmed by intensity dependent PL measurements. The intensity increase of both the near band edge transitions and the 2.1 eV emission was measured by varying the excitation intensity. As expected for strongly localized states the intensity increase followed a power law with an exponent below 1 ($I \sim L^{0.95}$) for the deep level emission and above 1 ($I \sim L^{1.2}$) for delocalized states as typically involved in the near band gap emissions [111].

Detailed analysis of the red luminescence at 2.1 eV revealed that this band was a convolution of at least three different transitions, indicated by the full and dashed arrows in the topmost spectrum of Fig. 21. The energy differences between the main peak and the two low energy peaks correspond nearly exactly to the binding energies of the omnipresent shallow acceptor (E_A=129 meV) and to the binding energy of the shallow carbon acceptor (E_A^C = 215 meV), respectively. Therefore, the red luminescence was attributed to a superposition of three transitions involving the same deep defect level E_{Deep} located 1.185 eV below the conduction band. Since the electrical measurements on C-doped cubic GaN samples showed also a clear reduction of the free hole concentration at C-fluxes above $8x10^{10}cm^{-2}s^{-1}$ the deep defect acts as a deep donor [90].

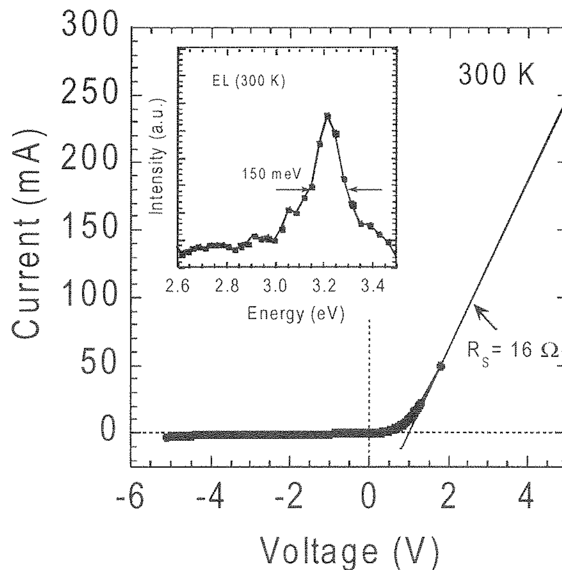

Figure 21. The room temperature current-voltage curve of a c-GaN p-n$^+$ junction. The inset shows the room temperature electroluminescence (current = 150 mA) of this diode emitted through a semitransparent Au contact.

The nature of the deep compensating complex is still unclear. As already mentioned earlier Kaufmann *et al.* [56] observed similar phenomena for Mg-doped MOVPE GaN layers and proposed self-compensation via the formation of nearest neighbor $Mg_{Ga}V_N$ pairs. However, C is placed on a N site and the formation of a comparable defect C_NV_N, which is a second nearest neighbor pair, is unlikely. For cubic GaN:C, it is more tempting to apply an analogy to C doped GaAs. In GaAs the formation of a compensating dicarbon split-interstitial center was observed at high carbon concentrations [112]. This complex involved one C atom on a As lattice site and another C atom shifted along the [100] direction [113], and acts as a double donor in GaAs. An equivalent defect in cubic GaN would also explain the sublinear decrease of the PL intensity at high C-fluxes which implies that at least more than one Carbon atom has to be involved in the newly formed deep C-complex.

Based on effective-mass-theory (EMT) the binding energy of the shallow acceptor can be determined by

$$E_A = \frac{13.58eV}{\varepsilon(0)^2} \cdot m_{hh} \cdot \gamma \tag{4}$$

where ε (0) is the static dielectric constant, m_{hh} is the heavy hole mass and γ is a correction factor which depends on the ratio of the light hole to heavy hole mass [108,114]. Using light hole and heavy hole masses of 0.18 m_0 and 0.75 m_0 for cubic GaN, the correction factor γ is 0.6 [114]. In EMT typically ε (0) is used. However, as pointed out by Orton [115] this should not hold for GaN, where the acceptor binding energies are comparable or even larger than the optical phonon frequencies. In cubic GaN LO and TO phonon frequencies are 92 meV and 67 meV, respectively [116]. In this case it should be more appropriate to use the high frequency dielectric constant ε (∞). Applying $\varepsilon(\infty)=5.35$ an acceptor binding energy $E_A = 0.213$ eV was obtained which is in excellent agreement with the experimental results and demonstrates that C indeed introduces a shallow acceptor in c-GaN.

In other cubic III-V compounds like GaAs, InP and GaP Carbon is the acceptor with the smallest central cell correction. The binding energy is usually close to Mg and increases in the sequence C, Mg, Zn and Cd [108]. The same sequence is verified in cubic GaN now since the binding energy of C is lower than that observed for the Mg acceptor in c-GaN by 15 meV [85]. Due to the higher crystal symmetry, the binding energy of the C acceptor in the cubic phase is also lower than the activation energy of C measured in hexagonal GaN [108].

3.3. Light emitting diodes

For the fabrication of cubic III-nitrides light-emitting diodes (LEDs) and laser diodes (LD) operating in the visible and UV, it is necesary to fabricate a p-n junction in this material. Blue emitting GaN based LD are key components for laser printing, high density optical memory and next generation digital versatile disk DVD [117,118] and will enable the production of full-color displays and a lot of further applications are expected [119]. Up to now, all commercial available GaN based LEDs have hexagonal III-nitrides. A GaN device grown on conducting GaAs substrates, however, will enable

easy device processing, which is compatible to the GaAs-based LED technology currently used in industry and therefore, will significantly reduce production costs. Recently, Yang *et al.* [120] reported the first electroluminescence of a cubic-phase GaN LED grown on GaAs (001) substrates by metal organic chemical vapor deposition (MOCVD). However, the electrical data reported for their device showed values of the ideality factor larger than 20 and turn-on voltages larger than 6 V, which were neither compatible to a p-n junction nor to a Schottky diode. In addition the emission of the device originated from a Mg-related deep recombination.

A diode fabricated by Mg and Si doping of MBE-grown c-GaN on n-type GaAs (001) has been reported by As *et al.* [121]. Current-voltage (I-V), capacitance-voltage (C-V), photoluminescence (PL) and electroluminescence (EL) measurements were used to characterize the c-GaN p-n homojunction at room temperature. The cubic GaN p-n homojunction structure consisted of a 760-nm-thick p-type GaN:Mg on top of a 500-nm-thick n-type GaN:Si. Te-doped n-type GaAs (001) with a free electron concentration of about $2x10^{18}$ cm^{-3} was used as substrate. The vertically structured diode was completed after evaporating electrodes on both the n-type GaAs substrate (Sn-contacts) and the p-type top layer (semitransparent two-layer Au contact).

The I-V characteristics of the diode structures was clearly rectifying [122]. Electroluminescence (EL) under dc-biased conditions was emitted through the semitransparent part of the p-type contact from the surface side of the device. Figure 21 shows the I-V characteristic of the structure measured at room temperature. The GaN n^+-p diode forward turn-on voltage was approximately 1.2 V, which was about the same as that measured in hexagonal GaN p-n junctions (1.2 V) [123] and was much lower than that observed by Yang *et al.* [120]. At a forward bias larger than 1.2 V the current grew linearly with the applied voltage. A fit to the I-V curve yielded a series resistance of 16 Ω, which is comparable to that reported for commercial III-V nitride LEDs [124]. Because of its large band-gap (3.2 eV), the reverse bias saturation current due to minority carrier diffusion would be immeasureably small in an ideal GaN p-n diode. However, significant reverse bias leakage was observed in c-GaN diodes, indicating the presence of trap levels within the band gap, which may act as a shunt or parallel conductance. At 5 V a dark current density of 0.25 A/cm^2 was measured. The large lattice mismatch between the GaAs substrate and c-GaN, which leads to a dislocation density in the order of 10^{11} cm^{-2} [81], may also be responsible for the high dark current.

The inset of Fig. 21 shows the electroluminescence of the c-GaN n^+-p junction through the semitransparent part of the p-type contact. The EL spectrum was peaked at 3.2 eV (387 nm) with an FWHM of 150 meV (20nm) and was nearly identical to the RT PL-spectrum, suggesting that in MBE grown c-GaN LED the dominating recombination processes are near band-edge transitions. This is in contrast to MOCVD grown cubic LED's where the emission originated from the blue Mg-related impurity mediated recombination [120]. Similar differences in the LED emission of MBE and MOCVD grown samples have also been reported for hexagonal GaN samples [125]. Due to the dominating near band transition the observed FWHM is also within the narrowest values ever reported for UV-LEDs. For the LED a linear increase of the intensity with increasing current density was measured and no shift of the EL-spectrum to lower energies was observed.

4. MBE of cubic InGaN

The growth of cubic GaN layers with excellent structural, optical and electrical properties (as demonstrated by the observation of optically stimulated emission at room temperature from cleaved c-GaN layers [126] and electroluminescence from a MBE grown c-GaN p-n junction [121]) has clearly demonstrated the potential of III-nitrides with cubic crystal structure for the realization of optoelectronic devices like light-emitting diodes and laser diodes. However, the bulk of experience accumulated with hexagonal III-nitrides shows that all working devices contain InGaN in the active region. The extensive utilization of InGaN in the active layer allows to tune the band gap energy and cover the short wavelength visible to near ultraviolet light spectrum. However, the incorporation of high amounts of In into the active region of h-InGaN-based emitters is still a serious problem. Although impressive progress has been achieved in addressing this problem the emission efficiency of emitters still drops significantly with increasing emission wavelength. Cubic GaN has a room temperature band gap of 3.2 eV, which is 0.2 eV smaller than that of hexagonal GaN. It has been expected that a similar relation holds also for c-InGaN and thus the availability of high-quality c-InGaN would open an attractive alternative to the hexagonal nitrides for the production of green and amber emitters. This was a strong motivation for c-III nitride growth.

Outstanding properties of hexagonal InGaN based devices are: (i) Unlike other III-V semiconductors in which defects of moderate density (as low as 10^5 cm^{-2}) reduce luminescence efficiency, III-nitrides exhibit very high luminescence efficiency in spite of the existance of dislocations with densities as high as 10^{10} cm^{-2}. (ii) A large Stokes-shift between emission and absorption energies exist in h-InGaN quantum wells and the Stokes-shift increases with increasing In-content of the layers.

The coexistance of a high quantum yield of photoluminescence and a high density of threading dislocations has been interpreted as being indicative for a strong localization of excitons in space. One current focus of research is to understand the mechanism of this localization. One possibility is the formation of InN quantum dots in the InGaN alloy [127-129]. The large difference in interatomic spacing between GaN and InN can give rise to a miscibility gap. Calculated phase diagrams of InN/GaN [130-132] reveal that at typical growth temperatures of 600 - 800°C, a strong tendency of InGaN layers exist to separate into regions of varying In-content. Another possibility is the localization caused by natural composition fluctuations in InGaN without clustering of In-atoms [133]. Exciton recombination in In-rich clusters can also explain the observed Stokes-shift in quantum wells. However, due to the low symmetry of the wurtzite lattice and the strain in pseudomorph quantum wells strong electric polarization fields can exist in h-InGaN quantum wells. These fields can effectively separate electrons and holes in quantum wells which may also result in a difference between the absorption and the emission wavelength (quantum-confined Stark effect).

The importance of submicrometer-scale chemical inhomogeneities of the InGaN quantum wells in addition to the effects of piezoelectric and spontaneous polarization fields has been discussed extensively [134]. However, a clear distinction between these two effects has not yet been achieved with hexagonal III-nitrides. Therefore, it has been suggested to investigate InGaN quantum wells with cubic crystal structure in

order to clarify the precise mechanism of band gap inhomogeneities and carrier localization.

Spontaneous polarization does not exist in crystals with cubic symmetry. Furthermore, cubic group III-nitride layered structures are grown on (001) oriented substrates so that piezoelectric fields in strained layers are parallel to the quantum well plane and the separation of electron-hole pairs at the well/barrier interfaces is suppressed. On the other hand, the cubic nitrides have the same next-neighbour configuration and almost identical bond length as their hexagonal counterparts. Since phase separation processes are mainly depending on the next-neighbour interaction and the GaN and InN bond length, the fluctuations of the chemical composition may be quite similar in hexagonal and cubic InGaN quantum wells of equal average In-content. Experimental results obtained with cubic III-nitride double heterostructures (DHs) and quantum wells (QWs) may therefore also be relevant for the understanding of light-emission processes in hexagonal III-nitrides.

4.1. Cubic InGaN-layers

Due to the large difference of the formation enthalpies of GaN and InN the growth of InGaN layers with sufficient structural perfection is much more difficult than that of GaN. The high nitrogen vapour pressure over InN results in a small In-incorporation rate at those temperatures, which are usually used for GaN growth. Lower temperatures on the other hand can lead to poor crystal quality, most likely due to segregation of In onto the growth front. The difficulties of In-incorporation in InGaN are also reflected by the extremely strong temperature variation of the In sticking coefficient which has been measured in MBE experiments [135]. Figure 22 shows the sticking coefficient of In on c-InGaN as a function of the layer temperature. Reasonable In mole fractions in the layers can only be achieved at growth temperatures of less than 650°C and a sufficiently high In/Ga flux ratio. The In-rich growth front does not allow to observe any surface reconstruction by RHEED which prevents the in situ control of the growth regime. The MBE of c-InGaN layers with a well defined In-content therefore depends on the precise measurement of the In-flux and the substrate temperature. Since the sticking coefficient varies by five orders of magnitude when the substrate temperature is raised from 600°C to 720°C, a variation of the substrate temperature of only 5°C results in a variation of the In content by a factor of two. As a consequence strong variations of the composition of InGaN layers due to small fluctuations of the substrate temperature must be expected.

Abernathy *et al.* [136] reported the first growth of c-$In_xGa_{1-x}N$ (x=0.07-1.0) layers by metal organic molecular beam epitaxy. The layers were grown at 500°C. X-ray diffraction and selected area diffraction patterns were used to distinguish between the hexagonal and cubic phase. They found that InN films grown at a rate of 70 Å/min were cubic while the ternaries contained both cubic and hexagonal phases. No optical data of the layers were reported. The reason for that was not explained. Most likely the high density of extended defects suppressed any radiative recombination.

By increasing the substrate temperature to T_s=620°C and the V-III flux ratio to 3, Yang *et al.* [28] were able to grow c-InGaN layers with In-contents up to 11% by dc-plasma assisted MBE. The relative high substrate temperatures were used to desorb In accumulated on the growth front. The composition of the layers was measured by X-ray diffraction and cross checked by Secondary Ion Mass Spectroscopy (SIMS). Low

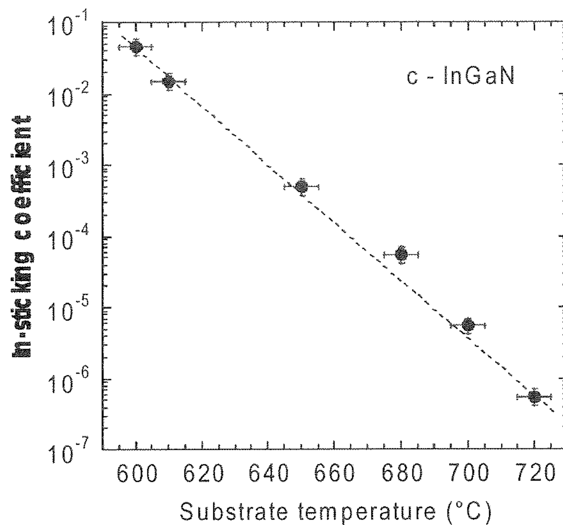

Figure 22. Sticking coefficient of In on a c-InGaN surface as a function of the substrate temperature. The Ga/N adatom ratio is constant and the In/Ga flux ratio is 100.

temperature photoluminescence (PL) was observed and the dependence of the emission energy on the composition of the InGaN layer was investigated. With increasing In-content the dominating PL peak was red-shifted and became both broader and weaker compared to the emission of layers with lower In-content. In the PL spectra of layers with $x>0.06$ a broad emission band at about 2.5-2.6 eV was observed which was tentatively attributed to deep level emission. Later investigations of c-InGaN layers with similar composition, however, revealed evidence that the emission at these energies is linked to the existence of QD-like structures [137].

Cubic InGaN layers with an higher In-content (up to $x = 0.4$) were grown by use of rf plasma sources providing a considerably higher nitrogen flux [138]. InGaN layers with an In-concentration of 17% exhibited blue luminescence at temperatures up to 500 K. The broad emission band had a maximum at about 2.8 eV. Layers with even higher In-concentration ($x = 0.4$) emitted luminescence in the green spectral region with a maximum at about 2.45 eV [139]. The intensity of the green emission decreased by only a factor of 4 when the temperature was raised from 4 to 400 K. Absorption and reflectivity measurements were used to determine the room temperature band gap energy of the InGaN layers yielding $E_{gap}=2.46\pm0.03$ eV which is close to the PL maximum. This correlation suggested that the PL stems from band edge related transitions in the InGaN layer. However, the weak temperature dependence of the intensity and the emission peak energy was rather consistent with radiative recombination between highly localized states. X-ray diffraction measurements of these layers revealed two Bragg reflexes, one due to the InGaN ($x=0.4$ layer) and a weak shoulder close to the position of the Bragg reflection of c-InN indicating the existence of an In-rich phase in these layers. It seems likely that the green emission band was also due to the recombination of excitons localized in In-rich clusters.

In order to clarify the appearing discrepancy more measurements of the gap energy were necessary. Goldhahn *et al.* [140] used spectroscopic ellipsometry to determine the complex refractive index of c-InGaN layers in the energy range from 1.5 to 4.0 eV. The c-InGaN layers were grown by plasma assisted MBE at a substrate temperature between 610 and 680°C on top of a c-GaN/GaAs hybrid substrate. The InGaN layers had a thickness of 100 to 200 nm. Their alloy composition was obtained from the lattice parameter measured by high resolution X-ray diffraction and by Rutherford backscattering (RBS) [79]. The InGaN layers were fully relaxed. This was inferred from reciprocal space maps of the symmetric (002) and the asymmetric (-1-1 3) Bragg reflexes and from RHEED reflex measurements during growth.

Figure 23 shows the room temperature gap energy of five c-InGaN layers. The circles are the result of spectrometric ellipsometry, the triangles are the results of transmission measurements [138,139]. The experimental data were fitted by a parabolic expression of the gap energy versus In-content (full curve) using a bowing parameter b=1.4 eV. This value is slightly higher than that calculated by Wright *et al.* [141]. It is, however, strikingly lower than experimental results for the hexagonal alloy system where composition-independent bowing coefficients of 3.2 [142] and 3.8 eV [143] were found. A composition-dependent bowing parameter was reported by McCluskey [144], however, their data referred to the absorption threshold energy which is lower than the average band gap [145]. Supercell empirical pseudo potential calculations [146] demonstrated that a large composition-dependent band gap bowing coefficient can be explained by localization of the hole wave function which is resonant with the valence band. For increasing In-content the effect is accompanied by a strong decrease of the

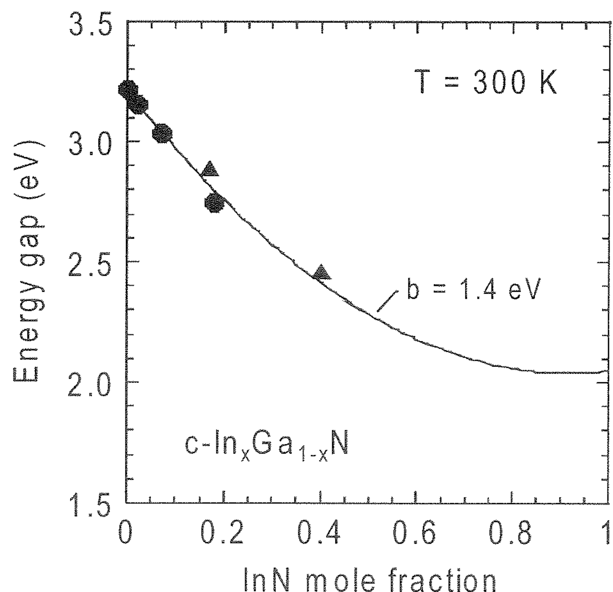

Figure 23. The room temperature energy gap of c-$In_xGa_{1-x}N$ versus InN mole fraction. Full dots represent data measured by spectroscopic ellipsometry [140] full triangles are results of Ref. 139. The full curve is a fit of the experimental data using a bowing factor b=1.4 eV.

momentum matrix element for transitions involving these In-related states. However, these transitions correspond rather to the absorption threshold than to the average band gap, which is measured by spectroscopic ellipsometry.

Low temperature photoluminescence (PL) spectra of the c-InGaN/GaN heterostructures are shown in Fig. 24 as full curves [147]. Luminescence was exited by the 325 nm radiation of a continuous-wave (cw) HeCd laser. The full width at half maximum (FWHM) of the InGaN layer emission increases from 200 meV to 450 meV with increasing x. The energy of the emission peak shifts to lower energies with increasing In content and is about 100-200 meV lower than the gap energy which was obtained from spectrally resolved ellipsometry.

The dashed curves in Fig. 24 are the spectra of light emitted from a cleaving edge of the heterostructure. In this case the InGaN layer surface was excited by the 340 nm light of a pulsed laser with an intensity of 1 MW/cm^2. The peak energy of the edge emission is shifted with respect to the luminescence peak close to the gap energy, indicating that localized states contribute to the PL at weak excitation. The localized states are filled by carriers with increasing excitation intensity and at 1 MW/cm^2 all low-energy radiative

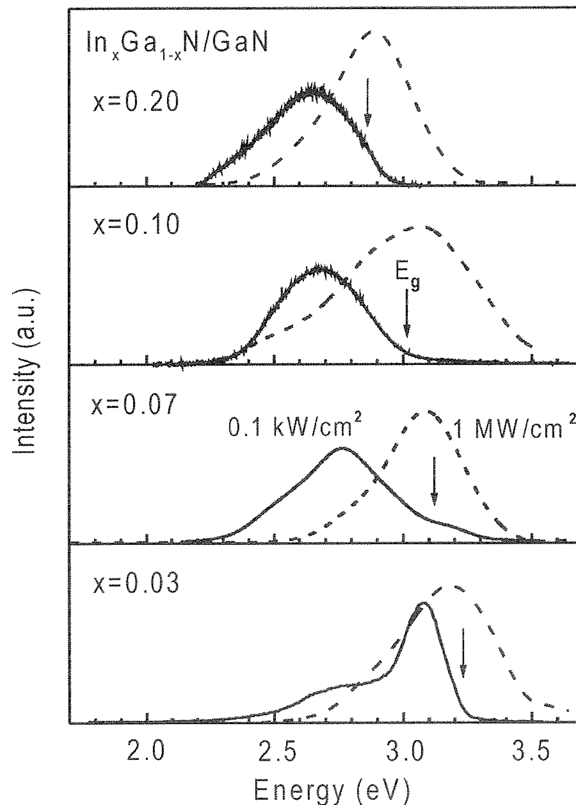

Figure 24. 2K photoluminescence spectra of c-In$_x$Ga$_{1-x}$N films (full curves) and the high-excitation edge emission (dashed curves). The gap energies from spectroscopic ellipsometry and reflectivity measurements are indicated by arrows.

recombination processes are saturated and the emission observed at high excitation is the near band edge luminescence from the InGaN layers. This suggestion is corroborated by time resolved measurements were a nonexponential decay of the PL was observed [147]. The kinetics of the recombination was described by the model of stretched exponentials which was introduced to describe the radiative decay of strongly disordered systems with localized recombination centres. It was applied successfully to h -InGaN [148], II-VI quantum dots [149], and porous Si [150].

Localization of excess electron-hole pairs has also a strong influence on the optical gain in c-InGaN layers. Figure 25 shows the gain spectra of an $In_{0.07}Ga_{0.93}N$ layer for excitation densities up to 5 MW/cm^2. With increasing excitation (i) the crossover between gain and absorption is shifted to higher energies, indicating the filling of the localized states, (ii) the gain structures broaden and (iii) the maximum gain shifts to higher energies. This behaviour is a further indication that the optical amplification is due to localized states because the gain of an electron-hole plasma is expected to shift to lower energies with increasing density [151]. Optical gain was observed up to 500 nm, indicating the advantage of c-InGaN for device applications in the green spectral range.

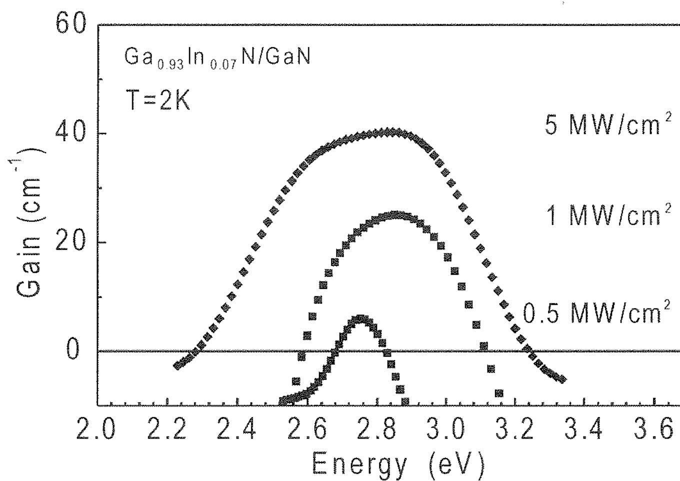

Figure 25. Gain spectra of a 280-nm-thick c-$In_{0.07}Ga_{0.93}N$ layer measured at various excitation intensities.

The correlation of structural and optical properties was further investigated by cathodoluminescence (CL) microscopy of c-InGaN layers with different In-content. The CL spectra of all c-InGaN layers exhibited broad emission bands, but their peak position changed according to the local composition. In samples with higher average In content (more than 10%) the fluctuations of the composition were strongly enhanced [152].

To monitor the influence of the of In content on the optical amplification, gain spectra of samples with varying In content were measured at a fixed excitation density of 7 MW/cm^2. Results are shown in of Fig. 26. The largest gain was observed for samples with an In content of about 7%, while for In contents above 20% the optical amplification was fully suppressed.

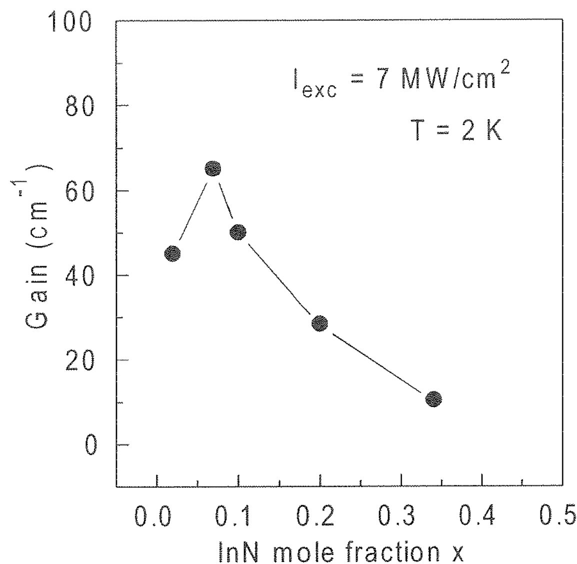

Figure 26. Peak gain of c-$In_xGa_{1-x}N$ layers measured at a excitation intensity of 7 MW/cm^2 versus InN mole fraction.

Evidence for phase separation in c-$In_xGa_{1-x}N$ layers was first obtained from investigations of their vibrational properties [153] using micro-Raman spectroscopy. The layers were grown on GaAs (001) substrates by plasma-assisted molecular beam epitaxy (MBE). Before starting the $In_xGa_{1-x}N$ growth a GaN buffer layer was grown on the GaAs substrate at a temperature of about 720°C. For the growth of the $In_xGa_{1-x}N$ layers, which had a thickness between 100 nm and 300 nm, the substrate temperature was decreased to 600-670°C.

Room temperature micro-Raman spectra of c-$In_xGa_{1-x}N$ layers are depicted in Fig. 27. The layers had an In-content of x = 0.07, 0.19 and 0.31 respectively. The composition of the layers was obtained by high resolution X-ray diffraction. Beside the TO and LO peaks of the layers (indicated by arrows in Fig. 27) the layer with x=0.31 showed an extra Raman peak at about 625 cm^{-1}. This peak was ascribed to the LO phonon mode of In-rich inclusions in the layer most likely formed by a phase separation process during growth. The existence of an In-rich phase was corroborated by X-ray diffraction, which showed that the c-InGaN layers contained strained crystalline cubic In-rich inclusions.

The electronic excitations of the In-rich phase in c-$In_xGa_{1-x}N$ layers were studied by resonant Raman scattering. [154] Raman spectra of c-$In_xGa_{1-x}N$ (x = 0.33), which were recorded at different excitation laser energies E_L are shown in Fig. 28. In the spectrum measured at E_L=2.81 eV, the LO and the weak TO phonon peak of the layer can be distinguished. By lowering the excitation energy a peak at about 630 cm^{-1}, indicated by S in Fig. 28 becomes evident and is further enhanced at even lower excitation energies. In the range of E_L between 2.5 eV and 2.34 eV, the S-peak becomes the strongest line in the spectrum. The integrated intensity of the S-peak as a function of excitation energy

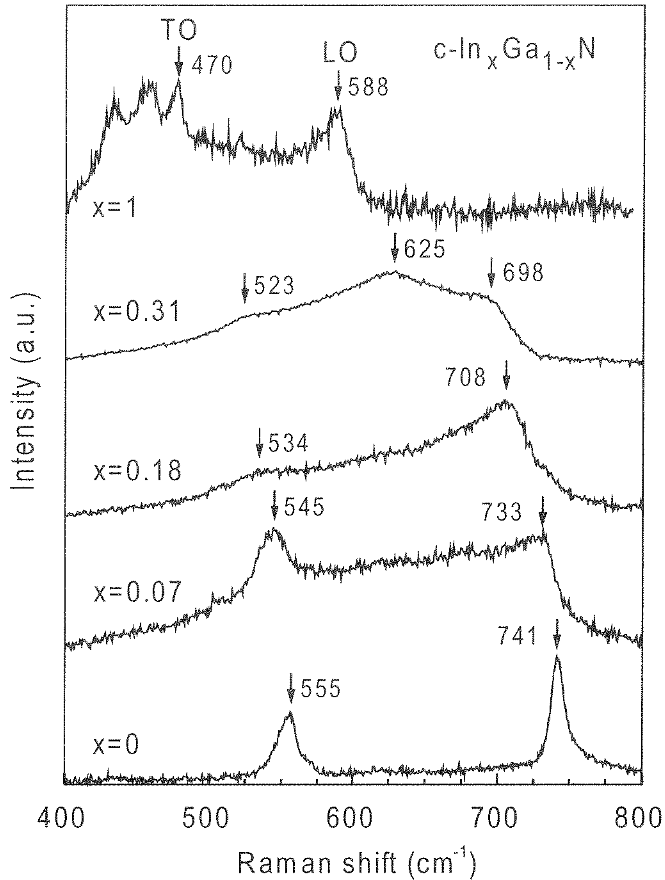

Figure 27. Room temperature micro-Raman spectra (excitation energy E_L=2.6 eV) of GaN, c-$In_xGa_{1-x}N$ layers with x = 0.07, 0.18, 0.33 and of c-InN.

E_L is shown in the inset of Fig. 28. The plot shows a clear resonance with a maximum at about 2.4 eV. Assuming that the maximum corresponds to an outgoing resonance process and taking into account the phonon energy of $In_xGa_{1-x}N$ (E_{LO}=78 meV) the energy of the resonant electronic excitation was calculated to be 2.32 eV. This value was in excellent agreement with the peak energy of the photoluminescence (PL) of the layer [137].

The photoluminescence spectra of c-InGaN layers with different In-content (x = 0.33, 0.19, 0.07) had peak energy close to the energy of the resonant Raman excitation energy of the S-peak (Fig. 28). PL emission at about 2.4 eV was also observed with c-$In_xGa_{1-x}N$ layers with an even higher In mole ratio (x = 0.4) [139] yielding evidence that the PL emission energy is widely independent of the nominal In-content of the layers.

It was supposed in Ref. 137 that the observed photoluminescence is due to radiative recombination of electron-hole pairs in In-rich regions of the layers. The composition of these regions was obtained by high resolution X-ray diffraction. By comparing the gap

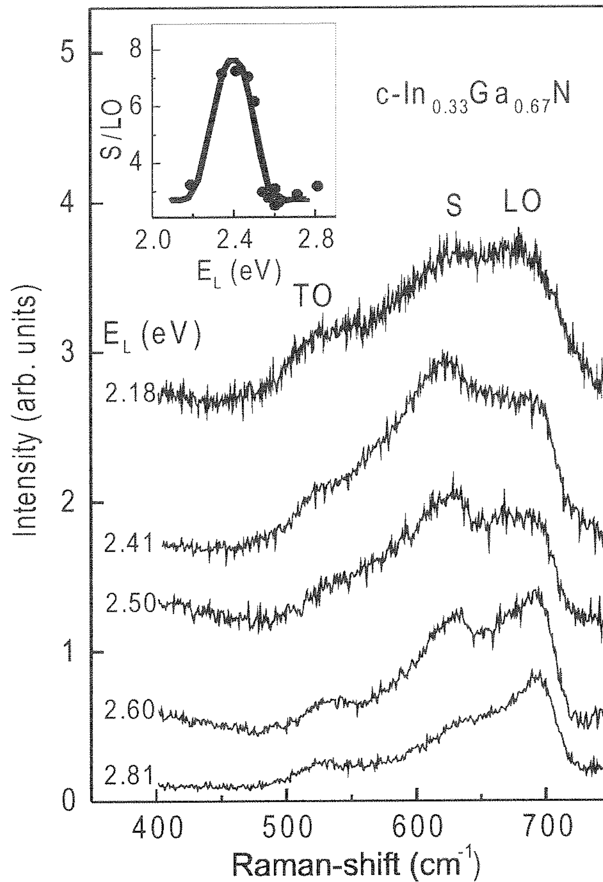

Figure 28. Room temperature micro-Raman spectra of c-$In_xGa_{1-x}N$ ($x = 0.33$). The energy of the exciting laser radiation E_L is indicated for each spectrum. The inset shows the ratio of the integrated intensity of the S and the LO peak as a function of the laser energy E_L.

energy of the In-rich phase and the measured optical transition energy it was found that the transition energy exceeds the gap energy by more than 100 meV. It has been concluded that this is due to confinement effects of quantum dot-like structures formed by phase separation in the c-$In_xGa_{1-x}N$ layers. From the confinement energy the size of these structures has been estimated to be about 3 nm using an effective mass model. These experiments demonstrated that the emission from c-$In_xGa_{1-x}N$ layers is associated with In-rich structures of nm-size formed by a self-organized process.

Recently Kitamura *et al.* [155] reported the MBE of c-InGaN layers on 3C-SiC(001)/GaN pseudo-substrates. A 7-μm-thick 3C-SiC(001) layers were grown by chemical vapor deposition on Si(001) wafers. After a 900°C heat treatment of the 3C-SiC surface a 10nm thick low temperature GaN buffer and a 300nm thick GaN layer were grown at 550°C and 760°C, respectively. The InGaN layers with a thickness between 200 nm and 450 nm were deposited at 640°C. The In/(In+Ga) flux ratio was

0.6-0.8, yielding a InN mole fraction between x = 0.05 and 0.2. High resolution X-ray diffraction (HRXRD) reciprocal space maps of the (113) Bragg reflex revealed that the 200nm thick layers were pseudomorphically strained on GaN, while the 450-nm-thick layers were fully relaxed. These results suggest that the critical thickness of cInGaN on 3C-SiC/GaN substrates is significantly larger than on GaAs/GaN, where InGaN layers of comparable composition but with a thickness of less than 100nm were fully relaxed [140]. The reason for this difference is not clear. It may be due to the substantially different conditions of the GaN surface in both growth regimes (see also Section 2.3).

The optical properties of the c-InGaN layers on 3C-SiC were characterized by PL, photoluminescence excitation spectroscopy (PLE) and time-resolved photoluminescence (TRPL) measurements [156]. With increasing InN mole fraction from 0.05 to 0.2 the PL emission energy decresed from 2.7 eV to 2.05 eV. These peak energies are significantly lower than those measured with c-InGaN layers on GaAs substrates and were red shifted with respect to the InGaN gap energy, which was obtained from PLE spectra. These spectra had a plateau-like region followed by a broad absorption tail at lower energies. The energy at which the PLE intensity started to decrease was defined as an effective gap energy. The gap energies measured in that way differ substantially from those which were obtained from spectrally resolved ellipsometry [157] and also the decrease of the gap energy with increasing In-content (bowing) was much more pronounced for c-InGaN on SiC than on GaAs. One reason for the appearing discrepancy may be the differing strain conditions on the respective layers, an other may be due to the methods used for the gap measurement.

TRPL experiments with c-InGaN on 3C-SiC revealed a non-exponential decay of the emission intensity. The decay was evaluated by the model of stretched exponents, yielding values for the initial decay time τ and the scaling parameter β which were almost identical to that obtained with InGaN layers on GaAs [147]. These data demonstrate that PL from c-InGaN layers is due to the recombination of electron-hole pairs which are trapped in localized states, independently of the substrate the layers are grown at.

4.2. Cubic-GaN/InGaN/GaN double heterostructures and quantum wells

In the following recent experimental investigations of c-GaN/InGaN/GaN double heterostructures (DH) and quantum wells (QW) are summarized. We shall compare DHs grown by MBE on GaAs(100) substrates with those on 3C-SiC. All reported investigations demonstrate clearly the strong influence of chemical inhomogeneities and In-segregation.

The DHs on GaAs(100) substrates [158] consisted of a 300-nm-thick GaN buffer layer grown under stoichiometric conditions at a substrate temperature of 720°C and a growth rate of about 40 nm/h. Then 30-nm-thick c-InGaN layers were deposited at a temperature of 600°C. During the InGaN growth the Ga-flux was reduced by about 20%. The variation of the In mol fraction in different samples was achieved by varying the In-flux between 0.5×10^{13} and 6×10^{13} atoms/$s^{-1}cm^{-2}$. A 30 nm GaN cap layer was finally grown at 600°C.

The lattice parameters and the strain in the DH structures were measured by high resolution X-ray diffraction. Figure 29 shows the distribution of the scattered X-ray

intensity in reciprocal space (reciprocal space map, RSM) of the asymmetric (-1-13) Bragg reflexes of two DHs. The InGaN layers were grown with an In flux of 6×10^{13} atoms/$s^{-1}cm^{-2}$ and 1×10^{13} atoms/$s^{-1}cm^{-2}$, respectively. Three maxima of the scattered X-ray intensity, one from c-GaN, one which was associated with the InGaN layer (InGaN(1)) and a weak reflex from an In-rich phase InGaN(2) are visible. Also included in the RSM are the calculated positions of the Bragg reflexes of c-GaN (a=0.452 nm), of c-InN, which is pseudomorphic (fully strained) to GaN and the position of the Bragg reflex of fully relaxed InN (a=0.497 nm) as well. The dashed lines indicate the position of Bragg reflexes of partially relaxed InGaN of a given composition (relaxation line). From the position of the InGaN related reflexes in Fig. 29 the composition of the InGaN(1) layers and of the InGaN(2) phase has been obtained.

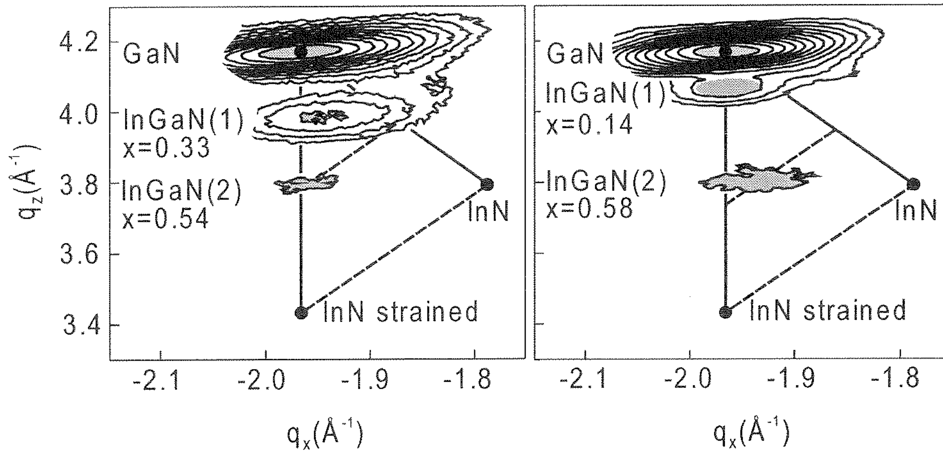

Figure 29. Reciprocal space maps of the asymmetric (-1-13) Bragg reflexes of two different c-GaN/InGaN/GaN double heterostructures. The curves show contours of equal intensity. The dots are the calculated positions of the GaN Bragg reflex and the Bragg reflex of fully relaxed and pseudomorph InN. The dashed lines are the relaxation lines of InGaN layers of a given composition.

Raman spectra of these DHs were recorded in backscattering geometry using laser light with an energy of 2.4 eV for excitation. The c-GaN phonon frequencies and two other peaks, corresponding to the LO phonon mode of the InGaN(1) layer and to LO phonons propagating in the In-rich InGaN(2) phase were clearly identified. The latter rather broad lines may alternatively also be due to disorder-induced Raman scattering. In fact a broad line at about 670 cm^{-1} has been observed with highly disordered GaN layers [159] which contained a large fraction (about 50%) of hexagonal inclusions, clearly visible in the Raman spectra from the coexistence of the cubic TO and an even more intense hexagonal E_2 phonon line. However, Raman and X-ray scattering revealed the phase purity of the DHs. Therefore disorder-induced scattering as the origin of the Raman peaks between 600 cm^{-1} and 700 cm^{-1} can be ruled out.

The fact that the LO phonon frequencies of c-InGaN vary linearly with x allowed to determine the InGaN alloy composition [153] revealing that the Raman results are in good agreement with the X-ray data [158].

Room temperature PL spectra of three different c-$In_xGa_{1-x}N$/GaN DHs are depicted in Fig. 30. Curve a) is a PL spectrum which was excited by HeCd laser radiation (E_L=3.81 eV) above the bandgap of c-GaN. The emission at 3.2 eV is due to excition recombination in the c-GaN barrier [67]. The emission bands at lower energy are also present in spectrum b) where E_L was well below the gap energy of GaN, indicating that this emission stems from c-InGaN. A Gaussian curve fit of the long wavelength part of the spectrum yields peak energies of 2.35 eV and 1.9 eV, respectively.

The PL emission from two other DHs with InGaN layers with a lower In-concentration (curves c, d) are also plotted in Fig. 30. It is a common feature of all these PL spectra that (i) the energy of the main emission peak is only slightly varying, and (ii) the gap energy of the In-rich InGaN (2) phase is below the energy of the dominating emission band. The latter may be inferred from the c-InGaN gap energies also shown in Fig. 30. They were obtained from the relation between Eg and the composition of relaxed c-InGaN layers [140] and the calculated gap shift due to biaxial compressive strain.

The weak PL at about 2.05 eV is only observed with samples grown at relatively high In-fluxes and may be due to radiative recombination in InN micro-crystals. Low temperature PL of c-InN was recently measured at about 2.1eV [160].

In order to explain these experimental data Husberg *et al.* [158] assumed that the observed luminescence at about 2.4 eV is due to the radiative recombination of excitons localized at In-rich, strained quantum-dot like structures which are embedded in the InGaN(1) layers. Since no spontaneous polarization- or piezoinduced electric fields exist in c-III-nitrides, the difference between the InGaN(2) gap and the luminescence peak energy is equal to the localization energy of the excitons E_{loc}. It was found that E_{loc} is decreasing with increasing In content of InGaN(1). In order to explain the variation, (i) an decrease of the localization energy due to the decrease of the confining potential V_0 which is equal to the difference of the band gap energies of the InGaN phases, and (ii) a variation of the size of the QDs were considered. In an effective mass model calculation of the ground state transition energy a three-dimensional quantum confinement structure in the form of a cube of dimension L was assumed, yielding that the QD structures have an average size of about 10 nm and the shift of the PL peak energy is mainly due to a decrease of the QD-size with decreasing In content of the layers. The influence of strain on the energy gap of InGaN alloys has been recently calculated more accurately [161]. If these values are used to obtain the average dot size, it is found to be about 3 nm smaller. More sophisticated ab-initio calculations of the InGaN QD energy gave an even smaller average dot size [162].

Kitamura *et al.* [155] fabricated cubic InGaN/GaN multi quantum well structures (MQWs) on 3C-SiC(001) substrates. Micrometer-thick 3C-SiC layers were grown by CVD on Si(001). Prior to GaN growth the SiC substrates were thermally cleaned at 900°C for 10 min. Then a low temperature GaN buffer and a 300-nm-thick GaN layer were grown at 550°C and 760°C, respectively. The MQW structures consisted of 5 InGaN/GaN periods. The c-GaN barrier and cap layer thickness was fixed at 10 nm and the InGaN well thickness L was varied from 0.6 to 10 nm. The InGaN layers were grown at 640°C.

The structures were characterized by high-resolution X-ray diffraction. The *c*-$In_{0.1}Ga_{0.9}N$ layers were pseudomorphically grown on relaxed *c*-GaN templates as confirmed by reciprocal lattice mapping of the multiplaye structures. Pronounced

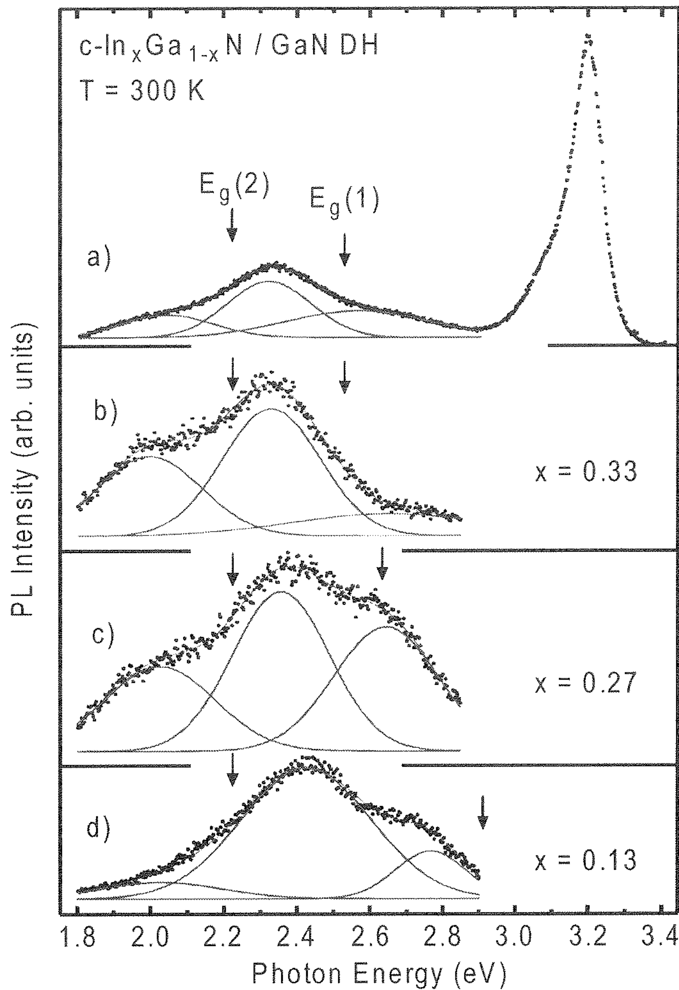

Figure 30. Room temperature PL spectra of c-InGaN/GaN double heterostructures with different In-content. Spectrum a) was excited above the gap energy of the GaN barrier, spectra b) to d) were excited below the GaN gap energy. The corresponding gap energies of the InGaN(1) and InGaN(2) phase are indicated.

satellite peaks due to the InGaN/GaN MQW were observed in ω-2θ XRD scans, revealing the high structural perfection of the structures. The InN mole fraction x was calculated from the strained lattice constants obtained from the XRD pattern and measured also by Auger electron spectroscopy of a fresh surface of the film.

The PL spectra of the c-$In_{0.1}Ga_{0.9}N$ MQWs measured at 77 and 300 K had a full width at half maximum of 250-300 meV, which is much larger than that of binary GaN [163]. The PL peak energy was nearly constant between 77 to 300 K. For $L<5$ nm the PL peak energy shifted to higher energy with decreasing L, which may be due to the quantum-size effect. The ground-state energy of excitons in a QW with a thickness L

was calculated by solving the Schrödinger equation using the values of an effective gap of the *c*-InGaN (x=0.1) film obtained from the PLE spectrum, which exhibited a plateau-like region followed by a broad absorption tail. The effective gap was defined as the energy at which the PLE intensity decreases to its half the maximum. The measured shift of the PL peak energy with **L** followed that of the QW resonance energy. In contrast to hexagonal-InGaN QWs, the PL peak energy increased moderately with decreasing L demonstrating the absence of an polarization-induced QCSE in *c*-InGaN QWs.

The TRPL signals from the 5-nm-thick c-$In_{0.1}Ga_{0.9}N$/c-GaN MQW showed a nonexponential decay at all temperatures similar to the case for *h*-InGaN bulk films and QWs, which is characteristic for the emission from localized states. The average lifetime was nearly independent of L and approximately 300 ps at 10 K. An evaluation of the radiative lifetime τ_r from PL-transients and the variation of the PL intensity with temperature revealed that τ_r increases linearly with increasing temperature above 150 K. From these findings it was concluded in Ref. 163 that excitons are localized in 2D structures. Quantum dot like structures, which were observed in relaxed c-InGaN layers and DHs [137,158] seem to be absent in fully strained c-InGaN/GaN QWs. This conclusion is in good agreement with recent investigations of strained and relaxed c-InGaN/GaN DHs grown on GaAs substrates which revealed that the formation of QD-like structures in InGaN is suppressed by strain in these layers [164].

4.3. Indium segregation and quantum dot formation

Experiments demonstrated the importance of exciton localization in c-InGaN layers, DHs and QWs due to nano-structural disorder as a result of composition modulation. Details of the formation process of these In-rich nano-structures are not clear yet. Theoretical models of the In-segregation process in InGaN layers have focussed on phase separation in the bulk (spinodal alloy decomposition). Calculated phase diagrams of bulk InGaN [130,131,132] revealed large miscibility gaps at those temperatures, which are applied for the epitaxial growth of InGaN layers. However, it is questionable if the assumption of thermodynamic equilibrium, which is made in these calculations, is valid for MBE growth. Bulk spinodal decomposition, which has frequently been observed with metallic alloys may also be hindered by the relatively slow self-diffusion in InGaN. Using experimental values of the In diffusion coefficient in h-InGaN [165] it is calculated that the In-atoms in our InGaN layers will diffuse less than 1 nm during the growth of the complete DH structure. This is obviously not sufficient to explain the formation of spatial fluctuation of the chemical composition on a nm-scale.

Another possible explanation for the formation of In-rich clusters is a separation of the alloy constituents at the surface during growth [166]. Since the In adatom mobility is quite high it seems reasonably to assume that In-rich clusters can aggregate in time intervals comparable to the time needed for the growth of one monolayer, and are buried then in the bulk of the layer because of the deposition of material. In this way fluctuations of the In-composition in the bulk may be formed. The spontaneous formation of In-clusters at the (0001) surface of h-InGaN by surface induced lateral composition modulations has recently be observed by tunneling microscopy [167]. It seems reasonable to assume that this process may also be active on cubic (001) surfaces.

Anneal experiments were performed to gain insight into the formation process of the In-rich phase in c-$In_xGa_{1-x}N$/GaN DHs [168]. The samples were annealed in vacuum for

10 hours. The annealing temperature was between 450°C and 700°C and was raised by 50°C for each annealing step. Subsequent to each anneal step PL and X-ray diffraction were measured. These annealing parameters were chosen in order to establish thermodynamic equilibrium at a temperature well above the growth temperature. This and the annealing time, which was ten times longer than the growth time of the InGaN layers yield an In diffusion length of several nanometer. A significant modification of the In-rich QDs can be expected if diffusion would not be hindered by other processes.

Figure 31 shows the PL spectrum of an as grown c-$In_xGa_{1-x}N$/GaN DH as well as spectra of the same sample annealed at 450°C and 700°C. All spectra were measured at room temperature with an excitation laser energy of E_L = 3.42 eV. The PL data in Fig. 31 clearly indicate that the spectral line shape and the energy of the emission at about 2.3 eV is not affected by the annealing procedure. Also X-ray diffraction data (RMS) show no detectable modification of the reflexes of the In-rich phase due to the annealing

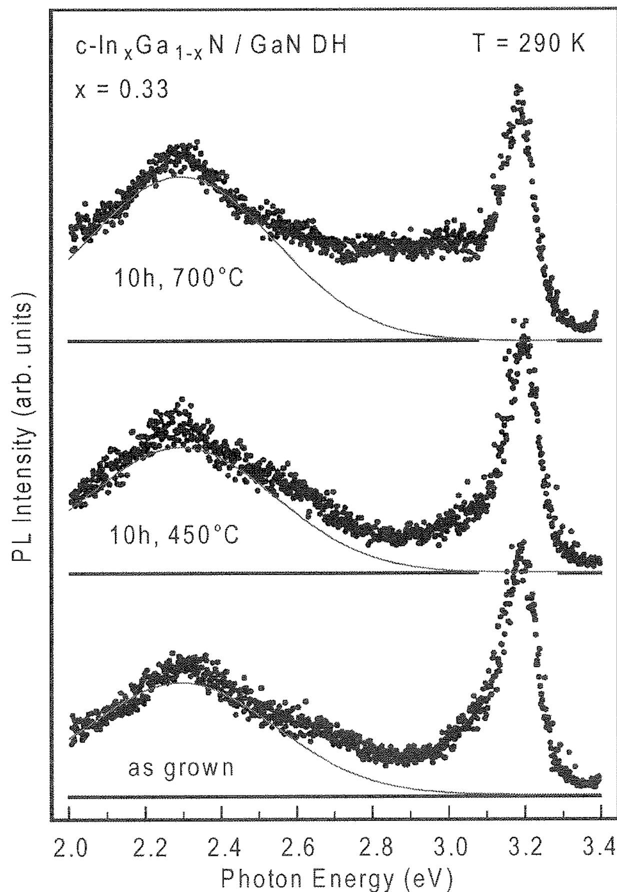

Figure 31. The room temperature PL of an as grown c-InGaN/GaN double heterostructure and the PL of the same sample after annealing for 10 hours in vacuum at temperatures of 450°C and 700°C, respectively. The PL emission from In-rich InGaN QDs is highlighted in the spectra.

procedure, revealing that composition and structure of the QDs are stable at annealing temperatures even above the growth temperature. These annealing experiments demonstrated that the process of formation of the In-rich phase is completed already during the growth procedure. They suggest also that InGaN layers with an uniform chemical composition can only be obtained when phase separation during growth can be avoided. This may be done either by applying sufficiently high growth rates, which may be difficult in MBE, however, or the growth of strained layers, since strain can suppress the phase separation process as recently proposed on the basis of theoretical calculations of the InGaN phase diagram [132] and demonstrated in experiment with c-InGaN/GaN DHs [164].

5. Conclusion

In this article we reviewed recent progress in the MBE of cubic III-nitrides. In spite of the inherent difficulties connected with the growth of compounds with metastable crystal structure, quite impressive progress has been achieved within the last years. This is in some part due to the possibility of in-situ control of the MBE process. The importance role the substrate plays for the MBE of c-III nitrides has been emphasized. From a technological point of view, GaAs seems to be the best choice, since it is cheap and available in large quantities. However, the large lattice misfit generates high dislocation densities in the c-III nitride layers and the small thermal stability of GaAs can cause problems in epitaxial growth at elevated substrate temperatures. For the future 3C-SiC seems to be the substrate of choice as demonstrated by recent experiments. Since spontaneous polarization and piezoelectric field due not exist in c-III nitrides, double heterostructures and quantum wells were considered as being optimally suited to clarify the origin of some peculiar properties of the luminescence from InGaN/GaN quantum wells. Experiments with MBE grown c-III nitrides have demonstrated the influence of quantum dot-like structures on photoluminescence emission from quantum structures. Doping is an inevitable prerequisite for any device application. Like in their hexagonal counterparts, high n-type conductivity in c-GaN can be achieved by doping with Si. For the MBE of c-GaN with p-type conduction doping by carbon seems to be an interesting new alternative to Mg-doping. Up to now, no commercial device application based on c-MBE-grown group III nitrides has been reported. To reach that goal some problems, which are mainly connected with the reduction of the density of extended defects in the c-III nitride layers, have to be solved. However, the observation of optical stimulated emission at room temperature from cleaved c-GaN layers and electroluminescence from c-GaN p-n junction has clearly demonstrated the potential of the c-III nitrides for future realisation of optoelectronic devices.

Acknowledgements

The authors acknowledge the support of this work by "Deutsche Forschungs-gemeinschaft" (DFG). We like to thank DAAD and PROBRAL for a long-termed and successful collaboration with the group of J.R. Leite at Sao Paulo University, Brazil.

References

1. Yeh, C.Y., Lu, Z.W., Froyen, S., and Zunger, A. 1992, Phys. Rev. B, **46**, 10086.
2. Paisley, M.J., Sitar, Z., Posthill, J.B., and Davis, R.F. 1989, J. Vac. Sci. Technol. A, **7**, 701.

3. Strite, S., Ruan, J., Li, Z., Manning, N., Salvador, A., Chen, H., Smith, D.J., Choyke, W.J., and Morkoç, H. 1991, J. Vac. Sci. Technol. B, **9**, 1924.
4. Okumura, H., Misawa, S., and Yoshida, S. 1991, Appl. Phys. Lett., **59**, 1059.
5. Lei, T., Fanciulli, M., Molnar, R.J., Moustakas, T.D., Graham, R.J., and Scanlon, J. 1991, Appl. Phys. Lett., **59**, 944.
6. Fujieda, S., and Matsumoto, Y. 1991, Jpn. J. Appl. Phys., **30**, L 1665.
7. Lei, T., Moustakas, T.D., Graham, R.J., He, Y., and Berkowitz, S.J. 1992, J. Appl. Phys., **71**, 4933.
8. Yoshida, S., Okumura, H., Misawa, S., and Sakuma, E. 1992, Surf. Sci., **267**, 50.
9. Miyoshi, S., Onabe, K., Ohkouchi, N., Yaguchi, H., Ito, R., Fukatsu, S., and Shiraki, Y. 1992, J. Cryst. Growth, **124**, 439.
10. Lin, M.E., Xue, G., Zhou, G.L., Greene, J.E., and Morkoç, H. 1993, Appl. Phys. Lett., **63**, 932.
11. Powell, R.C., Lee, N.E., Kim, Y.W., and Greene, J.E. 1993, J. Appl. Phys., **73**, 189.
12. Liu, H., Frenkel, A.C., Kim, J.G., and Park, R.M. 1993, J. Appl. Phys., **74**, 6124.
13. Okumura, H., Misawa, S., Okahisa, T., and Yoshida, S. 1994, J. Cryst. Growth, **136**, 361.
14. Kikuchi, A., Hoshi, H., and Kishino, K. 1994, Jpn. J. Appl. Phys., **33**, 688.
15. Nagahara, M., Miyoshi, S., Yaguchi, H., Onabe, K., Shiraki, Y., and Ito, R. 1994, Jpn. J. Appl. Phys., **33**, 694.
16. He, Z.Q., Ding, X.M., Hou, X.Y., and Wang, X. 1994, Appl. Phys. Lett., **64**, 315.
17. Kuznia, J.N., Yang, J.W., Chen, Q.C., Krishnankutty, S., and Khan, M.A. 1994, Appl. Phys. Lett., **65**, 2407.
18. Kim, J.G., Frenkel, A.C., Lie, H., and Park, R.M. 1994, Appl. Phys. Lett., **65**, 91.
19. Cheng, T.S., Jenkins, L.C., Hooper, S.E., Foxon, C.T., Orton, J.W., and Lacklison, D.E. 1995, Appl. Phys. Lett., **66**, 1509.
20. Cheng, T.S., Jenkins, L.C., Hooper, S.E., Foxon, C.T., Orton, J.W., and Lacklison, D.E. 1995, Appl. Phys. Lett., **66**, 1509.
21. Mula, G., Adelmann, C., Moehl, S., Oullier, J., and Daudin, B. 2001, Phys. Rev. B, **64**, 195406.
22. Adelmann, C., Langer, R., Feuillet, G., and Daudin, B. 1999, Appl. Phys. Lett., **75**, 3518.
23. Martinez-Guerrero, E., Adelmann, C., Chabuel, F., Simon, J., Pelekanos, N.T., Mula, G., Daudin, B., Feuillet, G., and Mariette, H. 2000, Appl. Phys. Lett., **77**, 809.
24. Feuillet, G., Hamaguchi, H., Ohta, K., Hacke, P., Okumura, H., and Yoshida, S. 1997, Appl. Phys. Lett., **70**, 1025.
25. Okumura, H., Hamaguchi, H., Feuillet, G., Ishida, Y., and Yoshida, S. 1998, Appl. Phys. Lett., **72**, 3056.
26. Schikora, D., Hankeln, M., As, D.J., Lischka, K., Litz, T., Waag, A., Buhrow, T., and Henneberger, F. 1996, Phys. Rev. B, **54**, R8381.
27. Lima, A.P., Frey, T., Köhler, U., Wang, C., As, D.J., Lischka, K., and Schikora, D. 1999, J. Cryst. Growth, **197**, 31.
28. Yang, B., Brandt, O., Jenichen, B., Müllhäuser, J., and Ploog, K.H. 1997, J. Appl. Phys., **82**, 1918.
29. Shokhovets, S., Goldhahn, R., Cimalla, V., Cheng, T.S., and Foxon, C.T. 1998, J. Appl. Phys., **84**, 1561.
30. Yang, H., Brandt, O., Wassermeier, M., Behrend, J., Schönherr, H.P., and Ploog, K.H. 1996, Appl. Phys. Lett., **68**, 244.
31. Trampert, A., Brandt, O., Yang, H., and Ploog, K.H. 1997, Appl. Phys. Lett., **70**, 583.
32. Yang, B., Trampert, A., Brandt, O., Jenichen, B., and Ploog, K.H. 1998, J. Appl. Phys., **83**, 3800.
33. Pankove, J.I. 1987, Mater. Res. Soc. Symp. Proc., **97**, 409.
34. Vincett, P.S., Barlow, A., and Roberts, G.G. 1977, J. Appl. Phys., **48**, 3800.
35. Munir, Z.A., and Searcy, A.W. 1965, J.Chem.Phys., **42**, 4223.

36. Schikora, D., Widmer, T., Prott, C., Lischka, K., Machel, G., Schäfer, P., Luther, S., and Ortenberg, M.V. 1996, Solid State Electronics, **40**, 63.
37. Okumura, H., Miwasa, S., Okahisa, T., and Yoshida, S. 1994, J. Cryst. Growth, **136**, 361.
38. Kim, J.G., Frenkel, A.C., Liu, H., and Park, R.M. 1994, Appl. Phys. Lett., **65**, 91.
39. Molnar, R.J., and Moustakas, T.D. 1994, J. Appl. Phys., **76**, 4587.
40. Cho, S.H., Sakomoto, H., Akimoto, K., Okada, Y., and Kawabe, M. 1995, Jpn. J. Appl. Phys., **34**, L236.
41. Lin, M.L., Swerdlov, B.M., and Morkoc, H. 1993, Appl. Phys. Lett., **74**, 5038.
42. Cho, S.H., Okumura, H., and Akimoto, K. 2000, Appl. Phys. Lett., **76**, 3861.
43. Wu, X.H., Kapolnek, D., Tarsa, E.J., Heyening, B., Keller, S., Keller, B.P., Mishra, U.K., DenBars, S.P., and Speck, J.S. 1996, Appl. Phys. Lett, **68**, 1371.
44. Barabasi, A.L., and Satnley, H.E. 1995, *Fractal Concepts in surface growth*, Cambridge University Press, Cambridge.
45. Headrick, R.I., Kycia, S., Park, Y.K., Woll, A.R., and Brock, J.D. 1996, Phys. Rev. B, **54**, 14686.
46. Okumura, H., Ohta, K., Feuillet, G., Balakrishnan, K., Chichibu, S., Hamaguchi, H., Hacke, P., and Yoshida, S. 1997, J. Cryst. Growth, **178**, 113.
47. Tsao, J.Y., Brennan, T.M., Klemm, J.F., and Hammons, B.E. 1989, J. Vac. Sci. Technol. A, **7**, 2136.
48. As, D.J., Schikora, D., Greiner, A., Lübbers, M., Mimkes, J., and Lischka, K. 1996, Phys.Rev. B, **54**, R11118.
49. Neugebauer, J., Zywietz, Z., Scheffler, M., Northrup, J.E., and Van der Walle, C.G. 1998, Phys.Rev. Lett., **80**, 3097.
50. Schöttker, B., Kühler, J., As, D.J., Schikora, D., and Lischka, K. 1998, Materials Science Forum, **264-268**, 1173.
51. Zywietz, T., Neugebauer, J., and Scheffler, M. 1998, Appl. Phys. Lett, **73**, 4.
52. Neugebauer, J., private communication.
53. Adelmann, C., Langer, R., Martinez-Guerrero, E., Mariette, H., Feuillet, G., and Daudin, B. 1999, J. Appl. Phys., **86**, 4322.
54. Morkoç, H. 1999, *Nitride Semiconductors and Devices*, Springer, Berlin.
55. Schubert, E.F. 1993, *Doping of III-V Semiconductors*, University Press, Cambridge.
56. Kaufmann, U., Schlotter, P., Obloh, H., Köhler, K., and Maier, M. 2000, Phys. Rev. B, **62**, 10867.
57. Guha, S., Bojarczuk, N.A., and Cardone, F. 1997, Appl. Phys. Lett., **71**, 1685.
58. Ber, B.Y., Kudriavtsev, Y.A., Merkulov, A.V., Novikov, S.V., Lacklison, D.E., Orton, J.W., Cheng, T.S., and Foxon, C.T. 1998, Semicond. Sci. Technol., **13**, 71.
59. Shimizu, S., and Sonoda, S. 2000, Proc. IW on Nitride Semiconductors (IWN2000), Nagoya, Japan, IPAP Conf. Series, **C1**, 740.
60. Zhang, R., and Kuech, T.F. 1998, Appl. Phys. Lett., **72**, 1611.
61. Birkle, U., Fehrer, M., Kirchner, V., Einfeldt, S., Hommel, D., Strauf, S., Michler, P., and Gutowski, J. 1999, MRS Internet J. Nitride Semicond. Res., **4S1**, G5.6.
62. Abernathy, C.R., MacKenzie, J.D., Pearton, S.J., and Hobson, W.S. 1995, Appl. Phys. Lett., **66**, 1969.
63. As, D.J., Richter, R., Busch, J., Schöttker, B., Lübbers, M., Mimkes, J., Schikora, D., and Lischka, K. 2000, MRS Internet J. Nitride Semicond. Res., **5S1**, W3.81.
64. Martinez-Guerrero, E., Daudin, B., Feuillet, G., Mariette, H., Genuist, Y., Fanget, S., Philippe, A., Dubois, C., Bru-Chevallier, C., Guillot, G., Aboughe Nze, P., Chassagne, T., Monteil, Y., Gamez-Cuatzin, H., and Tardy, J. 2001, Mater. Sci. Eng. B, **82**, 59.
65. Li, Z.Q., Chen, H., Liu, H.F., Wan, L., Zhang, M.H., Huang, Q., Zhou, J.M., Yang, N., Tao, K., Han, Y.J., and Luo, Y. 2000, Appl. Phys. Lett., **76**, 3765.
66. Souchiere, J.L., and Binh, V.T. 1986, Surface Science, **168**, 52.
67. As, D.J., Schmilgus, F., Wang, C., Schöttker, B., Schikora, D., and Lischka, K. 1997, Appl.

Phys. Lett., **70**, 1311.
68. De-Sheng, J., Makita, Y., Ploog, K.H., and Queisser, H.J. 1982, J. Appl. Phys., **53**, 999.
69. Abramov, A.P., Abramova, I.N., Verbin, S.Y., Gerlovin, I.Y., Grigorév, S.R., Ignatév, I.V., Karimov, O.Z., Novikov, A.B., and Novikov, B.N. 1993, Semiconductors, **27**, 647.
70. Burstein, E. 1954, Phys. Rev., **83**, 632.
71. Casey, H.C., and Stern, F. 1976, J. Appl. Phys., **47**, 631.
72. Yoshikawa, M., Kunzer, M., Wagner, J., Obloh, H., Schlotter, P., Schmitt, R., Herres, N., and Kaufmann, U. 1999, J. Appl. Phys., **86**, 4400.
73. Fernandez, J.R.L., Moyses Araujo, C., Ferreira da Silva, A., Leite, J.R., Sernelius, B.E., Tabata, A., Abramof, E., Chitta, V.A., Persson, C., Ahuja, R., Pepe, I., As, D.J., Frey, T., Schikora, D., and Lischka, K. 2001, J. Cryst. Growth, **231**, 420.
74. Fernandez, J.R.L., Chitta, V.A., Abramof, E., Ferreira da Silva, A., Leite, J.R., Tabata, A., As, D.J., Frey, T., Schikora, D., and Lischka, K. 2000, Mater. Res. Soc. Symp. Proc., **595**, W3.40.
75. Look, D.C. 1989, *Electronic characterization of GaAs materials and devices*, Wiley, Chichester.
76. Weimann, N.G., Eastman, L.F., Doppalapudi, D., Ng, H.M., and Moustakas, T.D. 1998, J. Appl. Phys., **83**, 3656.
77. Look, D.C., and Sizelove, J.R. 1999, Phys. Rev. Lett., **82**, 1237.
78. Blumenau, A.T., Elsner, J., Jones, R., Heggie, M.I., Öberg, S., Frauenheim, T., and Briddon, P.R. 2000, J. Phys.: Condens. Matter, **12**, 10223.
79. Portmann, J., Haug, C., Brenn, R., Frey, T., Schöttker, B., and As, D.J. 1999, Nuclear Instruments and Methods in Physics Research B, **115**, 489.
80. Brenn, R., Jamieson, D.J., Cimmino, A., Lee, K.K., Frey, T., As, D.J., and Prawer, S. 2000, Nuclear Instruments and Methods B, **161-163**, 435.
81. As, D.J., and Lischka, K. 1999, Phys. Status Solidi A, **176**, 475.
82. Brandt, O., Yang, H., Kostial, H., and Ploog, K.H. 1996, Appl. Phys. Lett., **69**, 2707.
83. Ploog, K.H., and Brandt, O. 1998, J. Vac. Sci. Technol. A, **16**, 1609.
84. As, D.J. 1998, Phys. Status Solidi B, **210**, 445.
85. As, D.J. Simonsmeier, T., Schöttker, B., Frey, T., and Schikora, D. 1998, Appl. Phys. Lett., **73**, 1835.
86. As, D.J., Simonsmeier, T., Busch, J., Schöttker, B., Lübbers, M., Mimkes, J., Schikora, D., and Lischka, K. 1999, MRS Internet J. Nitride Semicond. Res., **4S1**, G.3.24.
87. Martinez-Guerrero, E., Bellet-Amalric, E., Martinet, L., Feuillet, G., Daudin, B., Mariette, H., Holliger, P., Dubois, C., Aboughe Nze, P., Chassagne, T., Ferro, G., and Monteil, Y. 2002, J. Appl. Phys., (in print).
88. Brandt, O. 1998, Cubic group III nitrides, in *Group III-Nitride Semiconductor Compounds*, B. Gil (Ed.), Clarendon Press, Oxford, 417.
89. As, D.J., and Köhler, U. 2001, J. Phys.: Condens. Matter, **13**, 8923.
90. As, D.J., Köhler, U., Lübbers, M., Mimkes, J., and Lischka, K. 2001, Phys. Status Solidi A, **188**, 699.
91. Köhler, U., Lübbers, M., Mimkes, J., and As, D.J. 2002, Physica B, **308-310**, 126.
92. As, D.J., Köhler, U., and Lischka, K. 2002, Mater. Res. Soc. Symp. Proc., **693**, (in print).
93. Kirchner, P.D., Woodall, J.M., Freeouf, J.L., Wolford, D.J., and Petit, G.D. 1981, J. Vac. Sci. Technol., **19**, 604.
94. Kim, W., Salvator, A., Bothkarev, A.E., Aktas, O., Mohammad, S.N., and Morkoç, H. 1996, Appl. Phys. Lett., **69**, 559.
95. Teles, L.K., Scolfaro, L.M.R., Leite, J.R., Ramos, L.E., Tabata, A., Castineira, J.L.P., and As, D.J. 1999, Phys. Status Solidi B, **216**, 541.
96. Neugebauer, J., and Van de Walle, C.G. 1996, Mater. Res. Soc. Symp. Proc., **395**, 645.
97. Leroux, M., Beaumont, B., Grandjean, N., Massies, J., and Gibart, P. 1997, Mater. Res. Soc. Symp. Proc., **449**, 695.

98. Eckey, L., von Gfug, U., Holst, J., Hoffmann, A., Schineller, B., Heime, K., Heuken, M., Schön, O., and Beccard, R. 1998, J. Cryst. Growth, **189/190**, 523.
99. Kaufmann, U., Kunzer, M., Maier, M., Obloh, H., Ramakrishnan, A., and Santic, B. 1998, Appl. Phys. Lett., **72**, 1326.
100. Neugebauer, J., and Van der Walle, C.G. 1999, J. Appl. Phys., **85**, 3003.
101. Marques, M., Ramos, L.E., Scolfaro, L.M.R., Teles, L.K., and Leite, J.R. 2000, in Proc. 25th Intern. Conf. Phys. Semicond. (ICPS 2000), Osaka, 1411.
102. Boguslawski, P., Briggs, E.L., and Bernholc, J. 1996, Appl. Phys. Lett., **69**, 233.
103. Boguslawski, P., and Bernholc, J. 1997, Phys. Rev. B, **56**, 9496.
104. Webb, J.B., Tang, H., Rolfe, S., and Bardwell, J.A. 1999, Appl. Phys. Lett., **75**, 953.
105. Kobayashi, Y., Scholz, F., and Kobayashi, N. 1997, Jpn. J. Appl. Phys., **36**, 2592.
106. Sato, M., 1996, Appl. Phys. Lett., **68**, 935.
107. Ogino, T., and Aoki, M. 1980, Jpn. J. Appl. Phys., **19**, 2395.
108. Fischer, S., Wetzel, C., Haller, E.E., and Meyer, B.K. 1995, Appl. Phys. Lett., **67**, 1298.
109. Yu, P.W., Park, C.S., and Kim, S.T. 2001, J. Appl. Phys., **89**, 1692.
110. Bebb, H.B., and Williams, E.W. 1972, *Photoluminescence I: Theory*, (Ed.), Academic Press, New York, 181.
111. Schmidt, T., Lischka, K., and Zulehner, W., 1992, Phys. Rev. B, **45**, 8989.
112. Cheong, B.-H., and Chang, K.J. 1994, Phys. Rev. B, **49**, 17436.
113. Wagner, J., Newman, R.C., Davidson, B.R., Westwater, S.P., Bullough, T.J., Joyce, T.B., Latham, C.D., Jones, R., and Öberg, S. 1997, Phys. Rev. Lett., **78**, 74.
114. Gel´mont, B.L., and Dyakonov, M.I. 1972, Sov. Phys. Semicond., **5**, 1905.
115. Orton, J.W. 1995, Semicond. Sci. Techn., **10**, 101
116. Siegle, H., Eckey, L., Hoffmann, A., Thomsen, C., Meyer, B.K., Schikora, D., Hankeln, M., and Lischka, K. 1995, Solid State Commun., **96**, 943.
117. Nakamura, S., and Fasol, G. 1997, *The Blue Laser Diode*, Springer, Berlin.
118. Orton, J.W., and Foxon, C.T. 1998, Rep. Prog. Phys., **61**, 1.
119. Strite, S., and Morkoç, H. 1992, J. Vac. Sci. Technol. B, **10**, 1237.
120. Yang, H., Zheng, L.H., Li, J.B., Wang, C., Xu, D.P., Wang, Y.T., Hu, X.W., and Han, P.D. 1999, Appl. Phys. Lett., **74**, 2498.
121. As, D.J., Richter, A., Busch, J., Lübbers, M., Mimkes, J., and Lischka, K. 2000, Appl. Phys. Lett., **76**, 13.
122. As, D.J., Richter, A., Busch, J., Lübbers, M., Mimkes, J., and Lischka, K. 2000, Phys. Status Solidi A, **180**, 369.
123. Kozodoy, P., Ibbetson, J.P., Marchard, H., Fini, P.T., Keller, S., Speck, J.S., DenBaars, S.P., and Mishra, U.K. 1998, Appl. Phys. Lett., **73**, 975.
124. Nakamura, S., Mukai, T., and Senoh, M. 1994, Appl. Phys. Lett., **64**, 1687.
125. Grandjean, N., Massies, J., Lorenzini, P., and Leroux, M. 1997, Electron. Lett., **33**, 2156.
126. Holst, J., Hoffmann, A., Broser, I., Schöttker, B., As, D.J., Schikora, D., and Lischka, K. 1999, Appl. Phys. Lett., **74**, 1966.
127. Chichibu, S., Azuhata, T., Sota, T., and Nakamura, S. 1997, Appl. Phys. Lett., **70**, 2822.
128. El-Masry, N.A., Piner, E.L., Liu, S.X., and Bedair, S.M. 1998, Appl. Phys. Lett., **72**, 40.
129. McCluskey, M.D., Romano, L.T., Krusor, B.S., Bour, D.P., Johnson, N.M., and Brennan, S. 1998, Appl. Phys. Lett., **72**, 1730.
130. Ho, I., and Stringfellow, G.B. 1996, Appl. Phys. Lett., **69**, 2701.
131. Saito, T., and Arakawa, Y. 1999, Phys. Rev. B, **60**, 1701.
132. Teles, L.K., Furthmüller, J., Scolfaro, L.M.R., Leite, J.R., and Bechstedt, F. 2000, Phys. Rev. B, **62**, 2475.
133. Wang, L.W., and Zunger, A. 1994, J. Chem. Phys., **100**, 2394.
134. Chichibu, S.F., Abare, A.C., Mack, M.P., Minsky, M.S., Deguchi, T., Cohen, D., Kozodoy, P., Fleischer, S.B., Keller, S., Speck, J.S., Bowers, J.E., Hu, E., Mishra, U.K., Coldren, L.A., DenBaars, S.P., Wada, K., Sota, T., and Nakamura, S. 1999, Mater. Sci. Eng. B, **59**, 298.

135. Frey, T. 2000, PhD thesis, University of Paderborn.
136. Abernathy, C.R., MacKenzie, J.D., Bharatan, S.R., Jones, K.S., and Pearton, S.J. 1995, Appl. Phys. Lett., **66**, 1632.
137. Lemos, V., Silveira, E., Leite, J.R., Tabata, A., Trentin, R., Scolfaro, L.M.R., Frey, T., As, D.J., Schikora, D., and Lischka, K. 2000, Phys. Rev. Lett., **84**, 3666.
138. Müllhäuser, J.R., Jenichen, B., Wassermeier, M., Brandt, O., and Ploog, K.H. 1997, Appl. Phys. Lett., **71**, 909.
139. Müllhäuser, J., Brandt, O., Trampert, A., Jenichen, B., and Ploog, K.H. 1998, Appl. Phys. Lett., **73**, 1230.
140. Goldhahn, R., Scheiner, J., Shokhovets, S., Frey, T., Köhler, U., As, D.J., and Lischka K. 2000, Appl. Phys. Lett., **76**, 291.
141. Wright, A.F., and Nelson, J.S. 1995, Appl. Phys. Lett., **66**, 3051.
142. Wetzel, C., Takeuchi, T., Yamaguchi, S., Katoh, H., Amano, H., and Akasaki, I. 1998, Appl. Phys. Lett., **73**, 1994.
143. Wagner, J., Ramakrishnan, A., Behr, D., Maier, M., Herres, N., Kunzer, M., Obloh, H., and Bachem, K.-H. 1999, MRS Internet J. Nitride Semicond. Res, **4SI**, G2.8.
144. McCluskey, M.D., Walle, C.G.V.d., Mater, C.P., Romano, L.T., and Johnson, N.M. 1998, Appl. Phys. Lett., **72**, 2725.
145. O'Donnell, K.P., Martin, R.W., and Middleton, P.G. 1999, Phys. Rev. Lett., **82**, 237.
146. Bellaiche, L., Mattila, T., Wang, L.-W., Wei, S.-H., and Zunger, A. 1999, Appl. Phys. Lett., **74**, 1842.
147. Holst, J., Hoffmann, A., Rudloff, D., Bertram, F., Riemann, T., Christen, J., Frey, T., As, D.J., Schikora, D., and Lischka, K. 2000, Appl. Phys. Lett., **76**, 2832.
148. Pophristic, M., Long, F.H., Tran, C., Ferguson, I., and R.F. Karlicek, J. 1998, Appl. Phys. Lett., **73**, 3550.
149. Chen, X., Henderson, B., and O'Donnell, K.P. 1992, Appl. Phys. Lett., **60**, 2672.
150. Pavesi, L., and Cheschin, M. 1993, Phys. Rev. B, **48**, 17625.
151. Holst, J., Eckey, L., Hoffmann, A., Broser, I., Schöttker, B., As, D.J., Schikora, D., and Lischka, K. 1998, Appl. Phys. Lett., **72**, 1439
152. Holst, J., Hoffmann, A., Broser, I., Rudloff, D., Bertram, F., Riemann, T., Christen, J., Frey, T., As, D.J., Schikora, D., and Lischka, K. 1999, Phys. Status Solidi B, **216**, 471.
153. Tabata, A., Leite, J.R., Lima, A.P., Silveira, E., Lemos, V., Frey, T., As, D.J., Schikora, D., and Lischka, K. 1999, Appl. Phys. Lett., **75**, 1095.
154. Silveira, E., Tabata, A., Leite, J.R., Trentin, R., Lemos, V., Frey, T., As, D.J., Schikora, D., and Lischka, K. 1999, Appl. Phys. Lett., **75**, 3602.
155. Kitamura, T., Cho, S.H., Ishida, Y., Ide, T., Shen, X.Q., Nakanishi, H., Chichibu, S., and Okumura, H. 2001, J. Cryst. Growth, **227-228**, 471.
156. Chichibu, S.F., Sugiyama, M., Kuroda, T., Tackeuchi, A., Kitamura, T., Nakanishi, H., Sota, T., DenBaars, S.P., Nakamura, S., Ishida, Y., and Okumura, H. 2001, Appl. Phys Lett., **79**, 3600.
157. Goldhahn, R., Scheiner, J., Shokhovets, S., Frey, T., Köhler, U., As, D.J., and Lischka, K. 1999, Phys. Status Solidi B, **216**, 265.
158. Husberg, O., Khartchenko, A., As, D.J., Vogelsang, H., Frey, T., Schikora, D., Lischka, K., Noriega, O.C., Tabata, A., and Leite, J.R. 2001, Appl. Phys. Lett., **79**, 1243.
159. Siegle, H., Loa, I., Thurian, P., Kaczmarczyk, G., Filippides, L., Hoffmann, A., Thomsen, C., Schikora, D., Hankeln, M., and Lischka, K. 1997, Zeitschrift f. physikalische Chemie, **200**, 187.
160. Yodo, T., Yona, H., Ando, H., Nosei, D., and Harada, Y. 2002, Appl. Phys. Lett., **80**, 968.
161. Teles, L.K., Furthmüller, J., Scolfaro, L.M.R., Leite, J.R., and Bechstedt, F. 2001, Phys. Rev. B, **63**, 085204.
162. Kent, P.R.C., and Zunger, A. 2001, Applied Physics Letters, **79**, 1977.

163. Chichibu, S.F., Sugiyama, M., Onuma, T., Kitamura, T., Nakanishi, H., Kuroda, T., Tackeuchi, A., Sota, T., Ishida, Y., and Okumura, H. 2001, Appl. Phys. Lett., **79**, 4319.
164. Tabata, A., Teles, L.K., Scolfaro, L.M.R., Leite, J.R., Khartchenko, A., Frey, T., As, D.J., Schikora, D., Lischka, K., Furthmüller, J., and Bechstedt, F. 2002, Appl. Phys. Lett., **80**, 769.
165. Chuo, C.-C., Lee, C.-M., and Chyi, J.-I. 2001, Appl. Phys. Lett., **78**, 314.
166. Leonard, F., and Desai, R.C. 1998, Phys. Rev. B, **57**, 4805.
167. Chan, H., Feenstra, R.M., Northrup, J.E., Zywietz, T., Neugebauer, J., and Greve, D.W. 2000, Phys. Rev. Lett., **85**, 1902.
168. Husberg, O., Kharchenko, A., Vogelsang, H., As, D.J., Lischka, K., Noriega, O.C., Tabata, A., Scolfaro, L.M.R., and Leite, J.R. 2002, Physica E, (to be published).
169. Brandt, O., Yang, H., Jenichen, B., Suzuki, Y., Däweritz, L., and Ploog, K.H. 1995, Phys. Rev. B, **52**, R2253.